DESIGN, CONSTRUCTION, AND TESTING OF THE ENHANCED MICRO PULSE LIDAR

by: David R. Wood, Jr. and Stephen K. Cox

Department of Atmospheric Science
Colorado State University
Fort Collins, CO 80523

Funding Agencies:

- National Aeronautics and Space Administration
  (Grant No. NAG 1-1704)
- Office of Naval Research
  (Contract No. N00014-91-J-1422)

Colorado State University

DEPARTMENT OF ATMOSPHERIC SCIENCE

PAPER NO. 659

"DESIGN, CONSTRUCTION, AND TESTING OF THE ENHANCED MICRO PULSE LIDAR"

David Romaine Wood, Jr. and Stephen K. Cox

Department of Atmospheric Science
Colorado State University
Fort Collins, CO 80523

Research Supported by

National Aeronautics and Space Administration (Grant #NAG 1-1704)
and
Office of Naval Research (Contract #N00014-91-J-1422)

November, 1997

Atmospheric Science Paper No. 659

ABSTRACT

DESIGN, CONSTRUCTION, AND TESTING OF THE ENHANCED MICRO PULSE LIDAR

For many years, the complexity and fragility of most lidar (an acronym for Light Detection and Ranging) systems have restricted their use in field operations. Recent technological developments have allowed for more compact and rugged designs which afford easy transportability. Such a system is the Micro Pulse Lidar (MPL) developed by the National Aeronautic and Space Administration (NASA). An important feature of the MPL is the eye-safe manner in which it is operated.

This document describes the Enhanced Micro Pulse Lidar (EMPL) which is based on the MPL design. The EMPL employs a higher powered laser but still can be operated in an eye-safe mode. A faster detector and new data collection system provide finer range resolution than standard MPL models. But, the most significant improvement is the addition of a user-programmable timing and control system which enables the user to optimize eye-safety, system power and range resolution for specific targets.

This thesis details the enhancements made to the NASA design. The construction and optical alignment procedures will be discussed. Issues pertaining to hardware and system software will be examined. Test data are presented as are suggestions for the system's further development.

ACKNOWLEDGEMENTS

We would like to thank Dr. James D. Spinhirne and Mr. V. Stanley Scott of the National Aeronautics and Space Administration (NASA) Goddard Space Flight Center for providing countless hours of technical support. Furthermore, we would like to express our gratitude to Dr. John M. Davis and Melissa Tucker for their continuing support.

This research was funded by NASA under contract number NAG 1-1704 and by the Office of Naval Research under contract number N00014-91-J-1422.

TABLE OF CONTENTS

Chapter 1

INTRODUCTION AND BACKGROUND

1.1 INTRODUCTION

Lidar, an acronym for LIght Detection And Ranging, has been a valuable tool in the study of the atmosphere since the invention of lasers in the early 1960s (for an interesting account of lidar development, see Collis and Russell, 1976). Lidar is the logical extension to its microwave predecessor the radar (RAdio Detection And Ranging). Both systems emit electromagnetic radiation and measure the returned amount scattered from a target. Since light is short wavelength radiation, lidar is well suited to the study of small, suspended particles in varying density profiles such as the atmosphere.

For many years, lidar systems have been too complex, temperamental and costly to be used in the routine unmanned data collection mode necessary for atmospheric studies (Carswell, 1983). This is especially true for those wishing to use lidar in field operations, since most lidars have been too large or delicate to be transported reliably. Also, many lidar systems lack eye-safe operating conditions which often limits their unattended use.

Recent developments in both laser, detector and electronic technologies have allowed for the design of much more compact and rugged systems. One such system is the National Aeronautic and Space Administration's (NASA) Micro Pulse Lidar, or MPL (Spinhirne, 1993), so-called because of the low transmitted pulse energy (tens of micro-joules). This allows, through prudent expansion of the transmitted beam, operation within

recognized laser eye-safety standards. The system can operate at a pulse repetition frequency of several kilohertz and utilizes a high quantum efficiency, photon-counting, silicon avalanche photodiode detector in the receiver.

The Department of Atmospheric Science at Colorado State University (CSU) has desired a rugged, compact lidar system to aid in the study of various atmospheric phenomena. With NASA's assistance, a system was designed and built based upon the MPL, but with several enhancements. The Enhanced Micro Pulse lidar (EMPL) employs a more powerful laser, faster detector, and finer range resolution than the original MPL. It also introduces a new feature, a programmable timing and control system.

This document will describe work done in the design, construction and testing of the EMPL. The enhancements will be itemized and differences with older MPL models will be discussed. The next section presents a brief review of the general topics of lidar.

1.2 LIDAR PRINCIPLES

A typical monostatic lidar configuration is illustrated in Figure 1.1. The transmitter section of the lidar usually consists of a laser and an additional optical circuit. The transmitter optics can include polarizing elements, collimators, spatial filters, and other components to process the transmitted light. The receiver section is composed of its own optics and a transducer to convert the incoming light into an electrical signal that can be monitored and/or recorded. Receiver optical circuits vary by application, but usually include a filter to limit the radiation on the detector to the desired wavelengths. Finally, since the transmitter and receiver share the same terminal aperture in the monostatic configuration (often a telescope), a transceiving circuit is necessary. One of the essential functions of the transceiving optics is to isolate the receiver from the intense transmitted energy pulse.

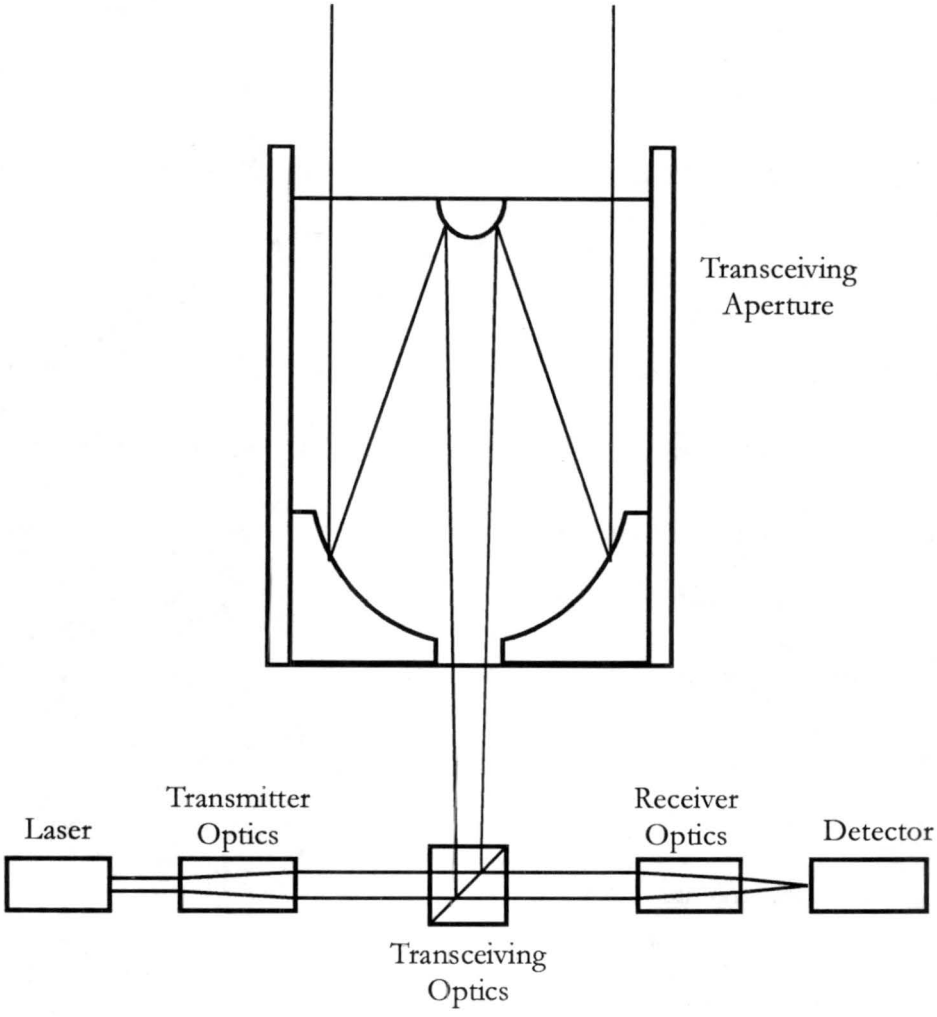

Figure 1.1 - The basic lidar configuration

In the case of pulsed lidar (and radar) systems, the transmitter releases a burst of electromagnetic energy. The energy interacts with objects in its path resulting in scattering of the radiation in various directions. The exact nature of the scattering mechanism is complex and highly dependent on the size of the target with respect to the wavelength of the incident radiation and its index of refraction. If the operating wavelength of the system is properly chosen based on the size of the object of interest, some of the energy scattered by the target will propagate towards the receiver where it may be detected.

One of the primary applications of the lidar is to acquire the backscatter profile of the atmosphere. This is possible because, in the single scattering case, the return power at the receiving aperture of atmospheric lidar is given by the basic lidar equation (Liou, 1980),

$$P_r = \frac{P_t A_r \beta_\pi(r) \Delta h T^2(r)}{8\pi r^2}$$

where P_t is the transmitted power, A_r is the area of the receiving aperture, $\beta_\pi(r)$ is the volume backscatter coefficient, Δh is the dimension of the scattering volume parallel to the path of the transmitted beam, and r is the range to the sample volume. The factor $T(r)$ is the atmospheric transmittance factor which accounts for the degradation of return power due to molecular absorption and scattering out of the sample volume. It is given by

$$T(r) = \exp\left(- \int_0^r \beta_e(r')dr' \right)$$

where $\beta_e(r)$ is the volume extinction coefficient. Note that the round trip transmission loss is $T^2(r)$. The volume backscatter coefficient, $\beta_\pi(r)$, relates the backward scattering efficiency of particles whose sizes are both above and below the Rayleigh limit and is often written as a sum, i.e.

$$\beta_\pi(r) = \beta_m(r) + \beta_p(r).$$

The subscripts m and p refer to molecular and particulate dimensions, respectively.

The complexity of actually extracting extinction or backscatter profiles by means of the basic lidar equation is often overlooked. The equation contains two unknowns when only one independent measurement is made. There are numerous mathematical inversion methods described in the literature such as Klett (1981), Kunz and de Leeuw (1993) and Young (1995). An inversion method using the MPL specifically has recently been modeled

by Cotturone and Cox (1996). All of these methods begin by range correcting the raw data, i.e.

$$X(r) = r^2 P(r)$$

and Young first removes the offset from background signal, detector dark current, etc. to produce,

$$X(r) = r^2\left(P(r) - P_0\right).$$

The inversion techniques are then applied to the resulting signal, $X(r)$.

The basic lidar equation neglects system losses and signal conversion for which the data must be compensated. For the MPL, the lidar equation in terms of a photon count rate, $n(r)$, is given by (Spinhirne, 1993) ,

$$n(r) = \frac{cE(r)A_r\eta_t\eta_r\eta_d J\left[\sigma_m(r) + \sigma_p(r)\right]T^2(r)}{2qr^2}$$

where c is the speed of light, $E(r)$ is transceiver geometric overlap factor, η_t and η_r are, respectively, the transmitter and receiver optical transmission efficiencies, η_d is the quantum efficiency of detector, J is the transmitted laser pulse energy, σ_m and σ_p are, respectively, molecular and particulate backscatter cross sections, and q is the photon energy. All other parameters are as described for the basic lidar equation. Spinhirne also defines the photon count rate from the background sky as

$$n_b = \frac{I(\lambda)A_r\eta_r\eta_d\Omega\,\Delta\lambda}{q}$$

where $I(\lambda)$ is the spectral radiance of the background, Ω is the solid angle field of view (FOV) of the receiver, and $\Delta\lambda$ is the receiver's optical bandwidth. However, n_b cannot be independently measured so a new quantity is defined,

$$n_o = n_b + n_c$$

where n_c is the dark count rate. The range corrected backscatter signal can then be obtained as

$$X(r) = r^2\left[n(r) - n_o\right].$$

It is in this fundamental form that data are displayed in real time for MPL[1] systems.

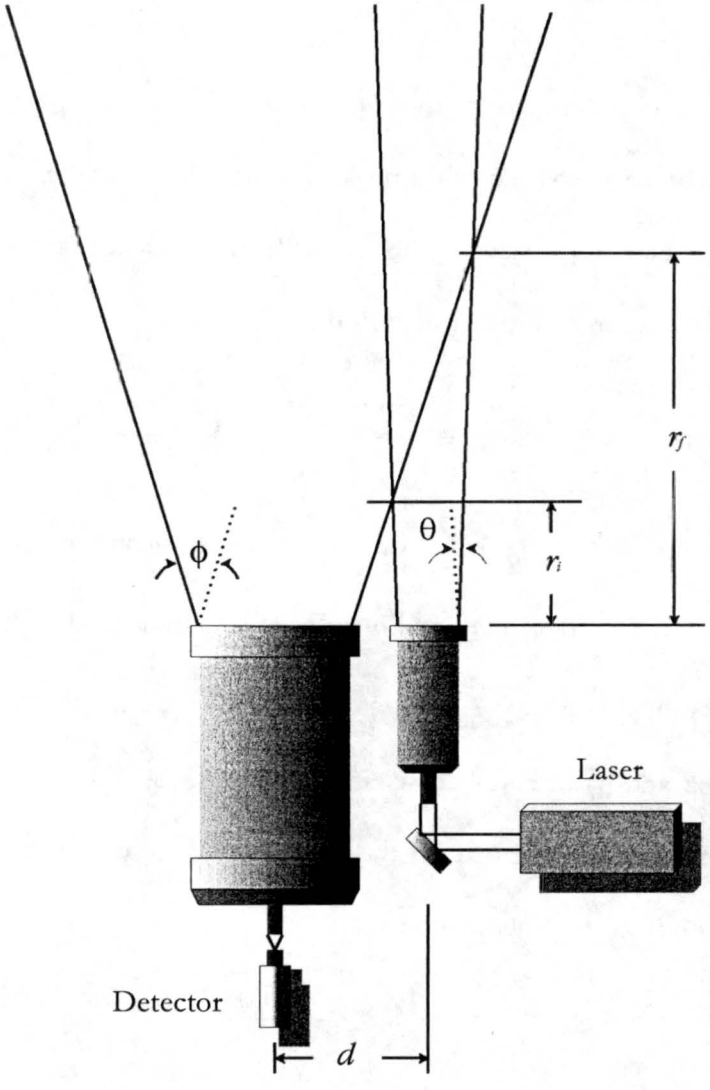

Figure 1.2 - The bistatic radar configuration demonstrating the geometric overlap between transmitter and receiver.

[1] Throughout this document, MPL will usually refer to both the original design and the EMPL unless it is otherwise clear from the context.

Once the MPL has been well calibrated, the system constants in the photon counting lidar equation can be easily compensated for. However, for the region of space close to the transceiving aperture, the receiver field of view may not coincide with that of the transmitter and the data must be adjusted. This is most easily visualized for the bistatic radar configuration as illustrated in Figure 1.2. In this arrangement, the axes of the transmitting and receiving apertures are separated by a distance *d*. The transmitter has a full angle FOV of θ and the receiver has a full angle FOV of ϕ. The FOV of an optical system is determined by its overall optical configuration and area of its field stop (Williams and Beckland, 1972). Since both transmitting and receiving systems have separate optical circuits, their fields of view could be different even if they share the same aperture.

After the transmitted pulse has traveled some distance, r_i, it begins to pass into the receiver's FOV. The maximum possible power can be received only if the entire transmitted pulse is within the receiver's FOV which occurs at range r_f. In the region between r_i and r_f, the geometric overlap correction factor, $E(r)$, can be applied to compensate for the loss of signal. The correction factor can be determined theoretically as in Harms (1979) or empirically. NASA uses a direct measurement method to determine the overlap correction factor for the MPL and that procedure is described in Appendix A.

For the MPL, the transmitting and receiving aperture is the same 20 cm Schmidt-Cassegrain telescope, but an overlap correction still needs to be applied for two reasons. First, as stated above, the transmitter and receiver utilize unlike optics and therefore have different fields of view. The second reason is due to the telescope design. The center of the aperture is obstructed by the secondary mirror. This causes a shadow on the detector

and therefore signal degradation at close range (Harms, 1979). At present, overlap correction for the EMPL has not been implemented. This will be explained in section 5.3.

1.3 EYE SAFETY

Personnel safety is, of course, an important consideration in the design and operation of lidar systems especially since the high energy density of most lasers can cause serious retinal damage. The MPL employs a low pulse energy laser, but to rarefy the laser's energy to satisfactory levels, the transmitted beam is expanded. Beam expansion is a common approach to achieve eye-safety especially when visible lasers are used. Other methods include the use of eye-safe lasers (wavelengths greater than 1.5 μm) or system shutdown when unexpectedly high return signals are detected (Matsui et al., 1994).

The recognized standard of laser eye-safety in this and other countries is ANSI Z136.1-1993. As the standard pertains to the MPL, the assumption is made that personnel will avoid intentional ocular contact. Furthermore, upon accidental viewing of the beam, a natural aversion response time of 0.25 seconds is assumed. With these understandings, the standard specifies that for a laser operating between 520 and 530 nm the Maximum Permissible Exposure (MPE) is 0.5 $\mu J/cm^2$. For pulsed lasers, the MPE must further be scaled by $N^{-0.25}$, where N is the number of pulses encountered in the 0.25 seconds of incidental contact.

To assess the safety of EMPL operations, the average laser power was measured with a power meter directly from the laser exit aperture and average pulse energy was found by dividing by the pulse repetition frequency (PRF). These data are depicted in the average power curve of Figure 1.3. In order to correctly compute the transmitted energy density it must be recognized that the transmitter aperture is blocked by the telescope's secondary mirror. If we assume that all the laser energy incident on the secondary mirror is reflected

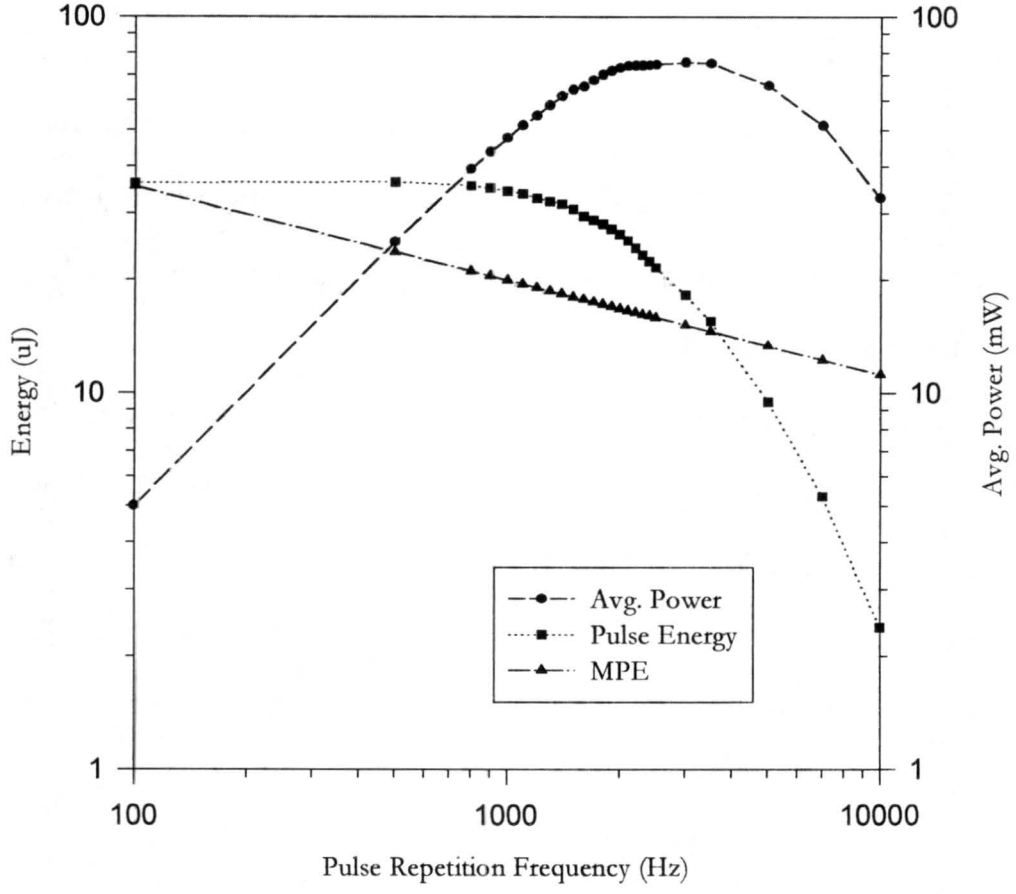

Figure 1.3 - Eye safe operation is at those frequencies where the MPE curve is above that of pulse energy.

onto the primary mirror and then exits the system, then the beam expansion is not the full 20 cm diameter of the telescope. The area to which the beam is actually expanded is 133.35 cm^2 which is the area of the 20 cm diameter aperture minus the area occupied by the secondary mirror. The pulse energy curve of Figure 1.3 was computed by applying a system transmission factor of 72.2% which excludes the telescope. The MPE curve follows the equation

$$0.5 \cdot [0.25 \cdot PRF]^{-0.25} \cdot 133.35 \quad \mu J$$

where 0.5 $\mu J/cm^2$ is the single-pulse MPE, the quantity in the brackets is the number of pulses in 0.25 seconds and the final factor is the 133.35 cm^2 area of expansion.

It is clear from Figure 1.3 that the transmitted pulse energy exceeds the MPE at the maximum average power frequency of 3.0 kHz. This is unfortunate since maximum average power results in the strongest look energy i.e. the energy transmitted for a fixed data-gathering period (Edde, 1993). There are, then, two options to operate the EMPL in an eye-safe mode. First, the optical pump to the laser can be decreased resulting in less per-pulse energy. Second, the EMPL can transmit at or above the 3.7 kHz point where the pulse energy falls below the MPE. The latter option is the most attractive since the average power does not fall off at a significant rate in that region. Since the EMPL employs a programmable timing and control system, either option can be selected with little effort.

Chapter 2

SYSTEM OVERVIEW

This chapter describes the EMPL system and discusses its subsystems. A block diagram of the system is depicted in Figure 2.1

2.1 OPTICAL TRANSCEIVER ASSEMBLY

The laser head and lidar optics are housed in the Optical Transceiver Assembly (OTA) a schematic diagram for which is given in Figure 2.2. This is the main system component and, basically, is the same optical assembly used in previous versions. In this section, a brief description of the operation and major components of the OTA will be given. First, since the correct operation of the OTA depends heavily on polarization, we will need to make a few definitions regarding orientation. For reasons that will become clear shortly, let us refer to the plane parallel to the OTA mounting plate as the receiver plane (p-polarized) and that which is perpendicular to the mounting plate as the transmitter plane (s-polarized). Note that the polarization tags 's' and 'p' are the industry standard referring to the polarization sense of light with respect to the plane of incidence on a boundary.

Upon command from the timing and control system, the laser head emits a polarized pulse oriented 45° to the OTA mounting plate. A half-wave retarding element is used to rotate the polarization to be parallel to the transmitter plane. The pulse then passes through a beam expander; an optical system which is basically a telescope in reverse. The divergence of a beam expanded in this manner is inversely proportional to the expansion

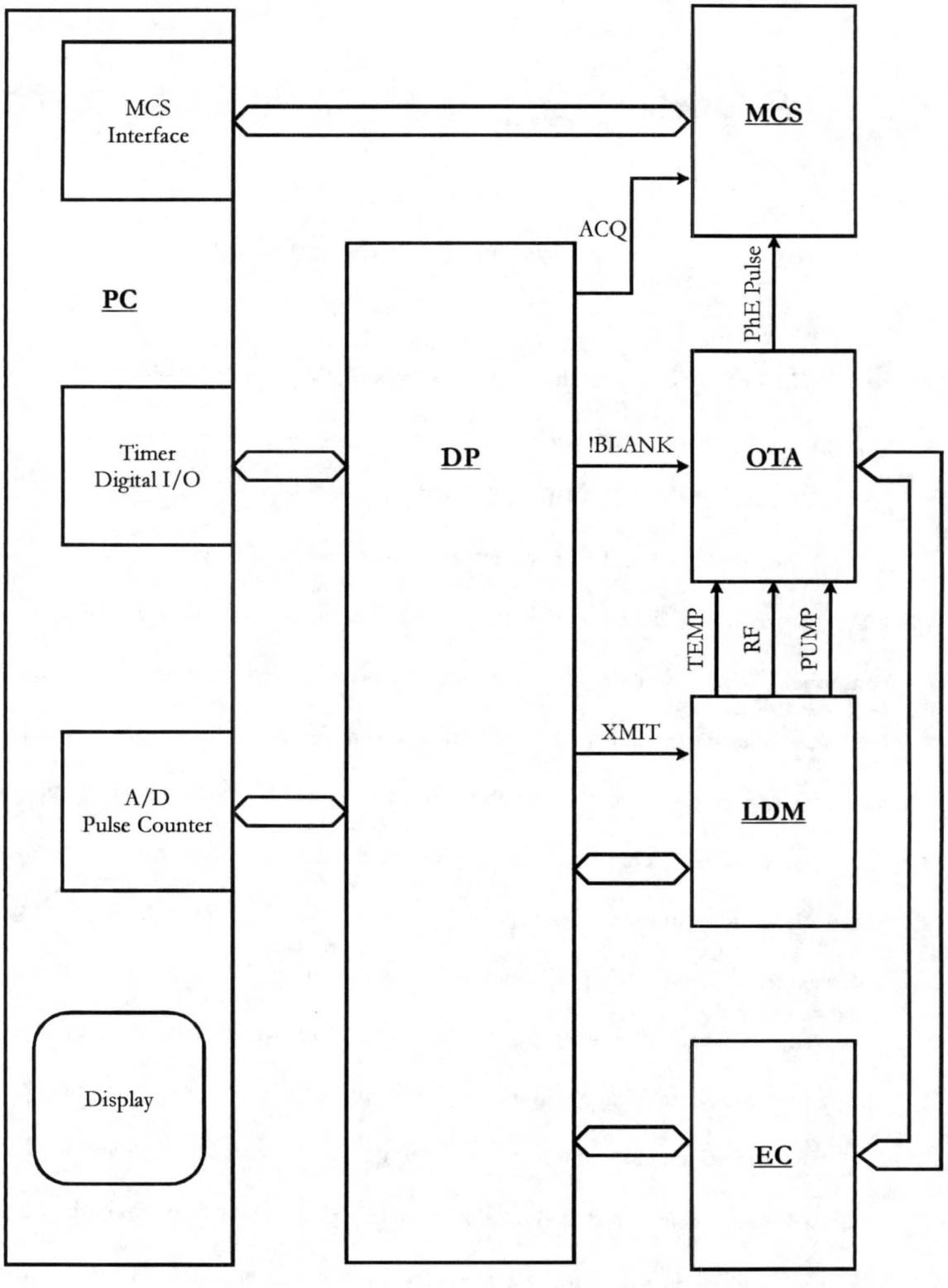

Figure 2.1 - The EMPL system.

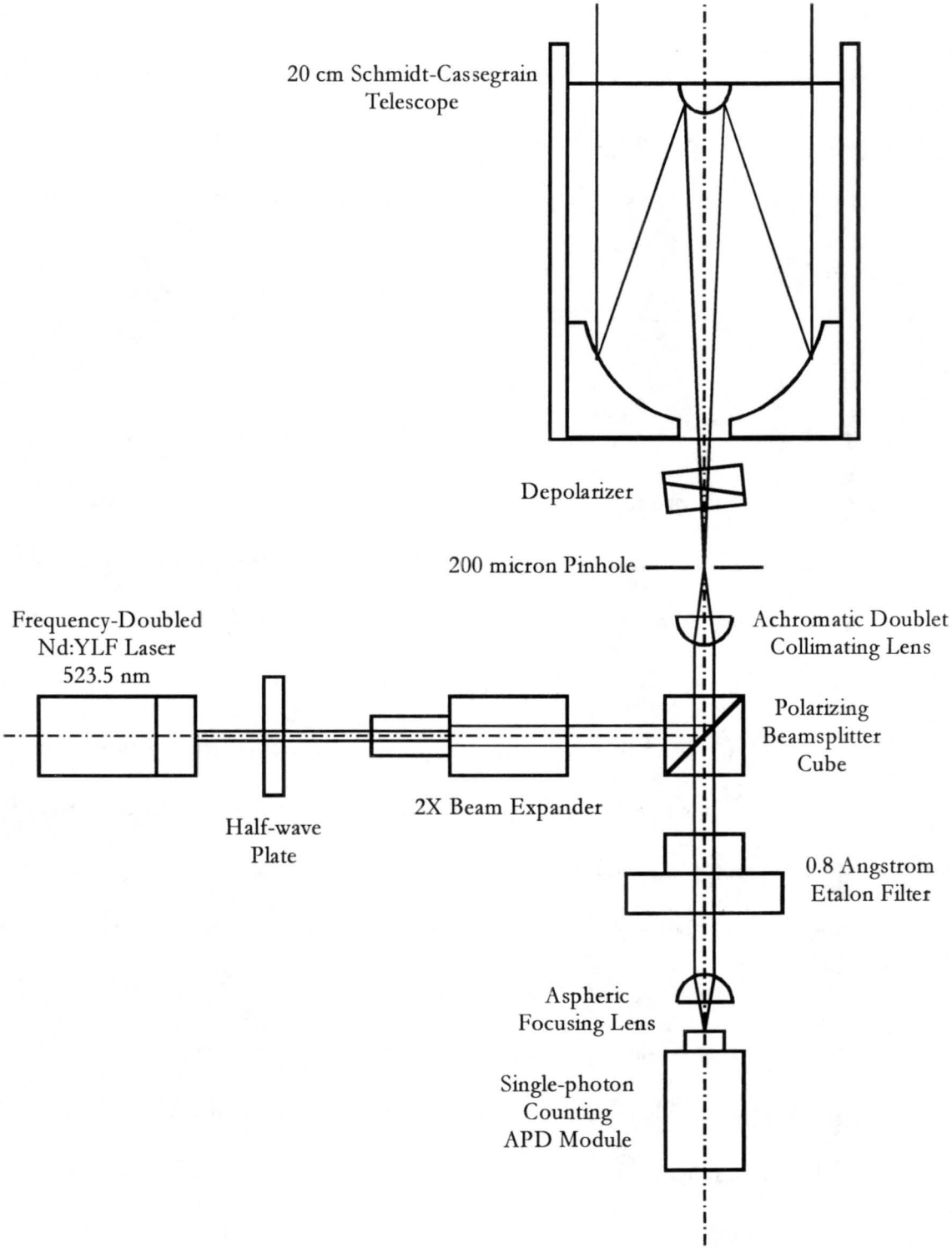

Figure 2.2 - The OTA optical schematic.

factor. Beam divergence can contribute to undesired aberrations in focusing optics, so collimation is the reason the expander is used in this application. The exit aperture of the beam expander is stopped down to prevent excess light from propagating through the rest of the system.

The laser pulse proceeds through optics that are shared by both the transmitter and receiver, i.e. the transceiver optical circuit. Therefore, the polarizing beamsplitter cube, the next element in the optical train, is one of the most critical in the entire OTA. Polarizing beamsplitter cubes are made of two right-triangular prisms optically joined with a film or gap at the interface. If the cube is properly constructed, unpolarized light normally incident on a cube face will be split into two orthogonally polarized beams. One beam passes straight through the device while the second beam is reflected and exits the cube 90° from the other beam. Let us define the amount of light transmitted straight through the cube as T_p and that which is reflected as T_s. Polarizing beamsplitter cubes are often specified by their extinction ratio, $\mathcal{Q}_p$, which is defined as T_p/T_s when the incident light is p-polarized. Similarly, we can define a new extinction ratio, $\mathcal{Q}_s$, as T_s/T_p when the incident light is s-polarized. The two quotients should be of the same order of magnitude for an efficient cube. It is critical that the cube used in the OTA have a high extinction ratio. The transmitted pulse is almost purely polarized in the transmitter plane and the great majority of it should be reflected at the interface of the cube. However, as it proceeds through the rest of the optical system, some of the light will be reflected back toward the cube and will most certainly become slightly depolarized. If the amount of depolarization is small and the cube has a large $\mathcal{Q}_s$, very little of the reflected light from the outgoing laser pulse will pass

straight through the cube and into the receiver. As will be discussed, an excess of light on the detector diminishes its performance.

The combination of the achromatic lens, pinhole, and telescope perform several essential functions. First, they provide the necessary beam expansion on the outgoing beam to assure eye-safety. Reciprocally, the elements form a focal reducer into the receiver as described by Schroeder (1987). The pinhole is located at the mutual focal point of the lens and telescope. It is used to limit the amount of light from rays arriving at the focal plane of the telescope but originating from off-axis points. Sources of this indirect component include light scattered from particles on the optics, off-axis background radiation, and multiple-scattered lidar returns.

Before the laser pulse is transmitted into the atmosphere, it must first be depolarized. Some particles do not change the polarization state of incident radiation (e.g. spherical water droplets). When backscattered from such particles, the transmitted beam will maintain its original polarization and be entirely reflected at the interface of the beamsplitter cube. That is to say, the returned light will take a path towards the transmitter rather than the receiver. By depolarizing the transmitted beam, at least some of the returned signal will be p-polarized and will pass through the beamsplitter cube and into the receiver. Although, true depolarization of polarized light is difficult and inefficient, several pseudo-depolarizers are commercially available. The element used in the MPL is a 3° wedge of crystal quartz which causes a variable phase delay across its face. If the area over which the depolarizer is illuminated is large, the exiting beam will effectively be depolarized (CVI, Unknown). A disadvantage of this design is that the wedge shape also causes deflection of the beam. To correct this, a similar wedge made of fused silica is mounted in optical contact to the quartz element (Temer, 1997).

Once the beam has been transmitted, light is returned to the system in a various polarization states. As previously discussed, some of the returned signal will be polarized parallel to the receiver plane and pass straight through the beamsplitter cube. It then encounters the first element of the receiver circuit which is the 0.8 Angstrom bandpass filter. The center of the passband is at the transmit wavelength of 523.5 nm. It is essential to have such a narrow band since the MPL's detector is sensitive to a relatively wide band of radiation. The increased level of background light in the receiver can seriously hamper the detection of the transmitted signal. The narrow band is achieved by employing an etalon which uses the principle of multiple beam interferometry (Hecht, 1987). A simple etalon could be built from two partially silvered mirrors separated a distance d by a material of index of refraction n. Assuming normal incidence, the device produces narrow fringes that obey,

$$2nd = \left(m + \frac{1}{2}\right)\lambda$$

where λ is wavelength. One can adjust n and/or d to locate one of the fringes at the desired wavelength. Then, to subdue the fringes on the long wavelength side of the MPL etalon, a multiple cavity blocking filter is used while those on the short wavelength side are blocked by an absorption filter. The critical spacing of the etalon is often maintained by a temperature-controlled *oven* in which the filter is mounted. A brief, but informative discussion of these narrow band interference filters can be found in the tutorial section of the Melles-Griot 1995-1996 optics catalog.

The signal entering the receiver is not only weak and poorly collimated, but it must be focused onto a 200 μm diameter spot. In order to capture all available light and direct it onto the detector, an aspheric focusing lens is installed in the receiver optical train. The

aspheric lens can replace a multi-element spherical lens system to provide high magnification in a smaller space. Also, a lens can be chosen with high numerical aperture (NA), i.e. (Hecht, 1987),

$$NA = n_0 \sin\theta_{\max}$$

where n_0 is the index of refraction of the surrounding medium (air in this case) and θ_{max} is the half-angle of the maximum cone for which light can enter the lens. If θ_{max} is large, marginal rays (light incident far from the axis of the lens) can contribute more to the signal than for a low NA lens.

Finally, the received light is incident on the photon counting avalanche photodiode (APD) detector module. The principles of photon detection by using an APD are neither new nor complicated (Ingerson et al., 1983). The classic example of how this is achieved is illustrated in Figure 2.3(a); the so-called passively quenched circuit (Oliver et al., 1993). The photodiode, D, is biased just slightly above its breakdown voltage. If the voltage across the device is high enough to provide a sufficient electric field, then an electron generated by an incident photon would be swept into the junction. The electron would accelerate under the influence of the electric field and undergo an ionizing collision with the silicon lattice thus creating an electron-hole pair (EHP). This process is called *carrier multiplication* and will continue as avalanche breakdown begins to occur. As more electrons are generated, more current begins to flow through the circuit. As a result, the voltage drop across the resistor, R, will increase until the diode's breakdown voltage can no longer be maintained and the avalanche current will be *quenched.* The resulting pulse at the node V_{out} generated by a single photon can be fed into a counter for photon-counting. Passively quenched photon-counting APDs can take microseconds to recover and during this *deadtime* are unable to process incoming photons. Therefore, they are limited to slowly occurring events. In cases

where higher incoming photon rates are expected, actively quenched APDs should be used. There are several circuit examples in the literature (Cova et al., 1982; Oliver et al., 1993; Dautet et al., 1993; Lacaita et al., 1995) and a simplified block diagram is shown in Figure 2.3(b). A detection circuit is used to sense the diode current. When the current crosses some threshold, the quenching circuit is activated. The sudden interruption of current usually causes the diode bias voltage to fall too far below its breakdown voltage, the recovery from which would introduce an undesirable delay. An added reset circuit is often used to quickly recharge the diode junction.

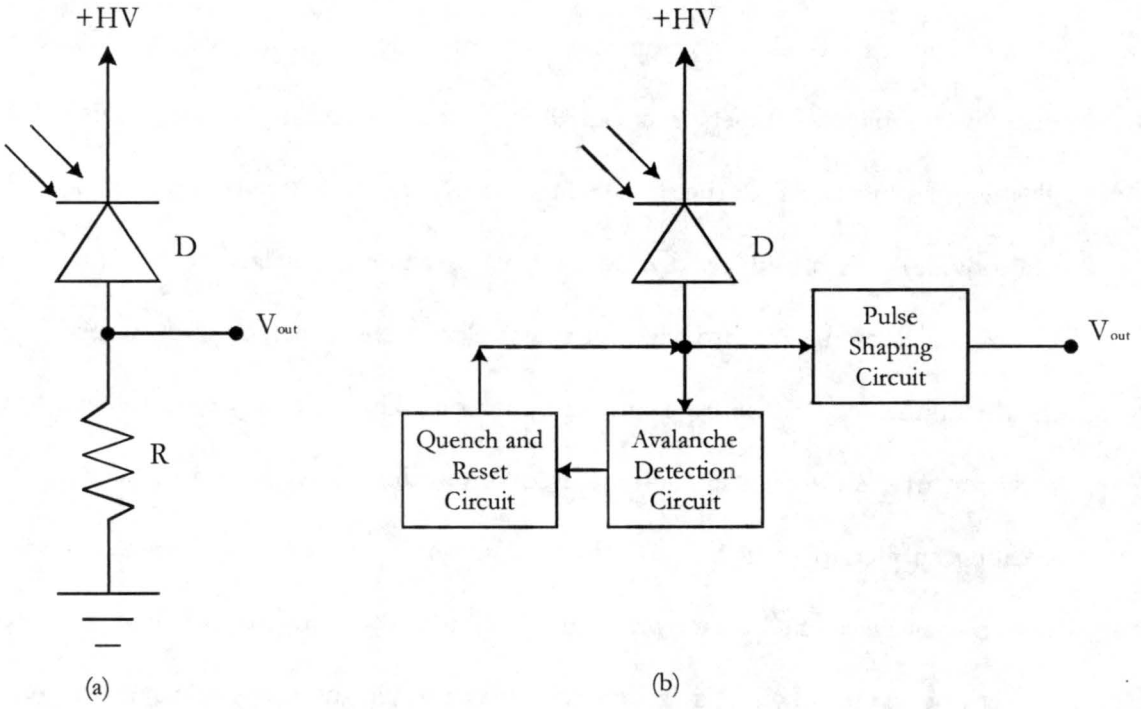

Figure 2.3 - Photon counting APD circuits.

The realization of a useful photon-counting system is not trivial. Thermally generated carriers can greatly outnumber those optically generated so the diode must be sufficiently cooled (Ingerson et al., 1983). Dautet et al. (1993) describe several limiting

value[3]. However, an excess of light (probably due to the transmitter pulse traversing misaligned optics) had reached the detector and caused the elevated rate. An example of what would normally be expected is given in Figure 2.5 the data for which were collected after the lidar optics were realigned. It is not known what physical processes in the detector cause the elevated count rate. The manufacturer of the module was consulted, but failed to identify a single cause. It is known, however, that when this occurs, the detector's performance is greatly diminished. Atmospheric phenomena such as optically thick clouds that should clearly be detected by the lidar are lost in the return signal.

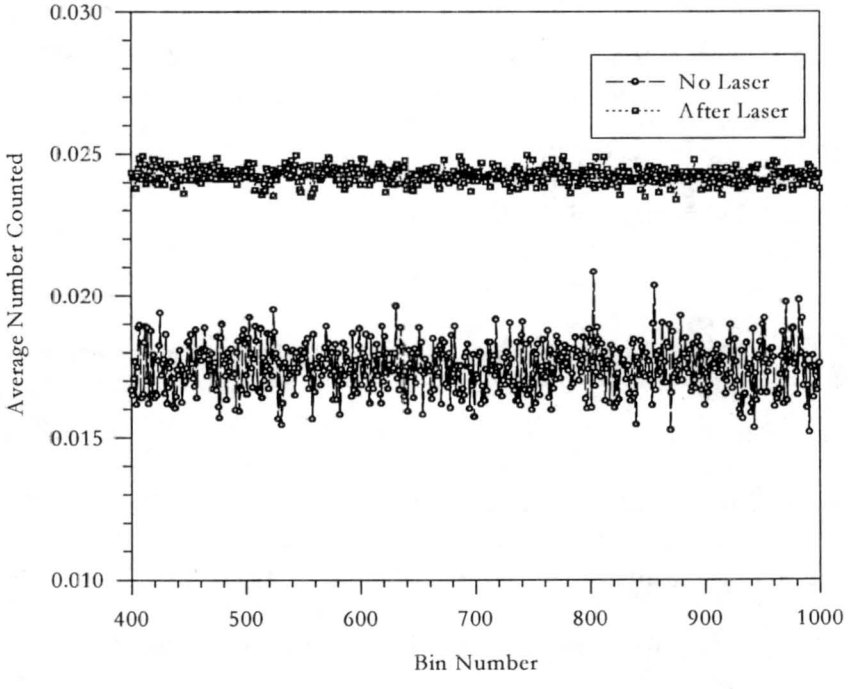

Figure 2.4 - An erroneously elevated count rate arising from excess light on the detector.

[3] Note that the difference in variance is due to an unequal number of integrations. More pulses were used for collecting backscatter data than were used for background data.

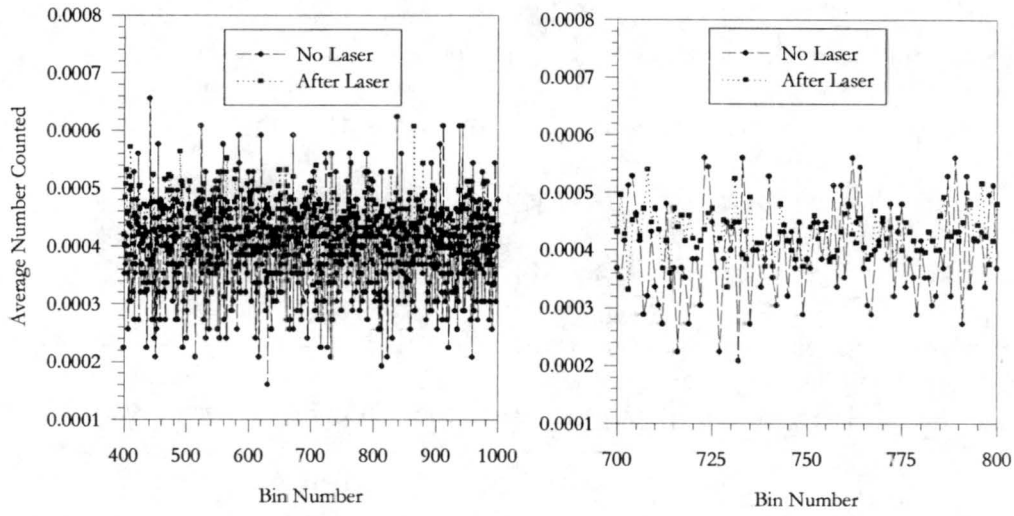

Figure 2.5 - The count rate for a correctly operating detector. The right panel is an expanded view of the left.

2.2 MULTICHANNEL SCALER

In the original design of the MPL, data are collected by means of a Multichannel Scaler (MCS). When an MCS scan begins, pulses at its input are counted into the first channel, or bin, until the specified dwell time has elapsed. It then begins to count into the next bin until the dwell time has again elapsed. This process is repeated until all channels have been counted into, whereupon the MCS is ready to perform the next scan. Data acquired during the new scan can either be added to or replace those of previous scans.

The output signal of the OTA is a stream of pulses corresponding to the number of received photons. The multichannel scaler allows the recording of the number of arriving photons as a function of time. By synchronizing the start of an MCS scan with the firing of a transmitter pulse and with the knowledge of the velocity of light, a backscatter profile of the atmosphere can be assembled.

The MCS used in previous MPL systems were chosen for their small size; occupying a single slot in a personal computer. However, the minimum channel width for those systems is 2μs corresponding to a 300 meter range resolution. The MCS used in the EMPL system is a much bigger desktop model, but its minimum bin length is 5 ns. Using a bin length less than 200 ns does, however, require special consideration for what is referred to as end-of-pass deadtime. This is the time required for the instrument to recover after each scan before it can begin the next. For the EG&G T914P, the MCS model chosen for the EMPL, this time is 360 μs + [150 ns × Number of Channels in a Pass]. Operating under this constraint would require decreasing the pulse repetition frequency from its optimum value of 3.0 kHz (the frequency that maximizes the average transmitted laser power). For channel widths of at least 200 ns, however, there is no end-of-pass deadtime. At present, 200 ns, which translates to a 30 m range resolution, is the default bin length for the EMPL.

2.3 LASER DRIVER MODULE

The laser head, which is located in the OTA, utilizes a neodymium-doped yttrium lithium fluoride (Nd:YLF) crystal as a lasing medium. The output of the laser is at 1047 nm but for this application, the radiation is frequency doubled producing a final wavelength of 523.5 nm. The laser head is optically pumped with two laser diodes via an optical fiber. The two pumping diodes are located in the Laser Driver Module (LDM) which also houses the temperature controller for the frequency-doubling crystal.

The laser pulses are formed by means of an acousto-optic Q-switch located at the output of the laser head. The Q-switch is a glass optical element bonded to a piezoelectric transducer. A radio frequency (RF) signal incident on the transducer causes an acoustic wave in the glass. The wave produces a change in the index of refraction allowing a build-

up of carriers in the Nd:YLF crystal. Lasing does not occur until the RF signal is removed from the transducer. The RF signal generator is located in the LDM.

2.4 EXPANSION CHASSIS

As the name implies, the Expansion Chassis (EC) provides space for future system expansion. At present, it contains the OTA temperature monitor circuits and the temperature controller and power supply for the etalon filter in the OTA receiver.

2.5 DISTRIBUTION PANEL

The Distribution Panel (DP) is the central hub of the system. It is where timing and control lines are directed to the appropriate subsystem. It houses line buffers as well as some timing circuitry, the details of which will be discussed in Chapter 4.

2.6 PERSONAL COMPUTER

The system is controlled by an i486 Personal Computer (PC). The PC contains the interface board which provides communication and data ingestion for the MCS. Also, an Omega Engineering CIO-DIO24/CTR3 Timer Digital I/O board provides the main system clock, some delay timing and system control. An Analog Devices RTI-815A Analog-to-Digital (A/D) Digital I/O board is used for temperature monitoring, laser control and transmitter pulse counting. The PC also provides the user interface and real-time data display. Details on both hardware and software aspects of the PC system will be revealed in Chapters 4 and 5.

Chapter 3

EMPL OPTICAL ASSEMBLY, ALIGNMENT, AND TESTING

In Chapter 2, a schematic diagram of the Optical Transceiver Assembly was presented. Although illustrative, the figure belies the physical layout of the optics and the challenges in the construction and alignment of the OTA. Much of the work requires special equipment which is not readily available. This chapter will discuss how the challenges were met and present some test results.

3.1 OPTICAL LAYOUT

The physical optical layout is depicted in Figure 3.1. The figure is a representation of a photograph in Appendix F and is not drawn to scale. One can now visualize the folded beam path which allows the OTA to be compact. The transmitted pulse exits the laser, passes through the half-wave plate and is incident on 45° Mirror 1. The beam is deflected 90° from its original path, passes through the beam expander and is redirected by Mirror 2. The beam is then incident on the beamsplitter and as explained in Chapter 2, it is almost totally reflected at the cube's interface. The beam is then guided onto the turning mirror (not shown in the figure but is clear in the photograph in Appendix F) which directs it into the rest of the transceiver circuit (into the page). The collimating lens, pinhole and depolarizer housing is screwed onto the visual back of the telescope (the port normally occupied by an eyepiece). The physical layout of the lens-pinhole-depolarizer assembly is

represented in Figure 3.2 and is also not drawn to scale. The beam passes through these elements and exits the OTA via the telescope.

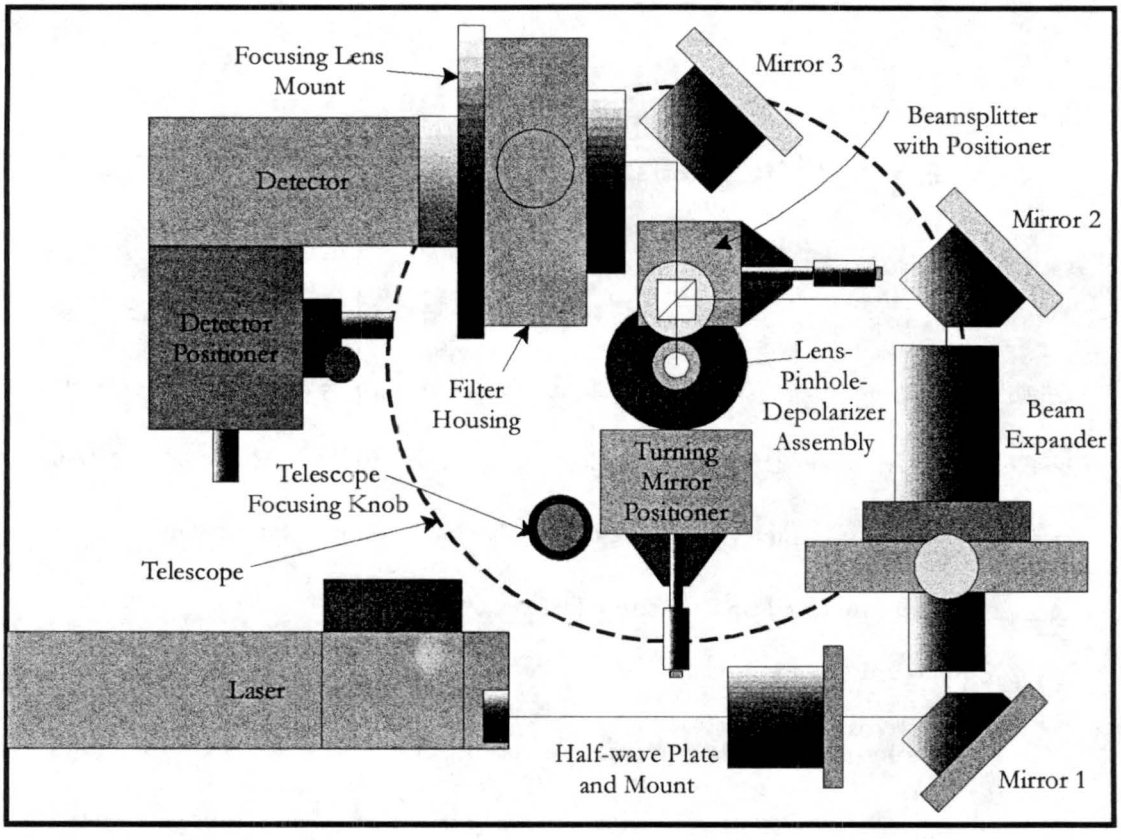

Figure 3.1 - OTA physical layout.

The backscattered signal enters the telescope and passes through the transceiver circuit. As previously explained, when the returned light strikes the beamsplitter, a portion of it will pass directly through the cube and the rest will take a path back through the transmitter circuit. The light that passes through the cube will be deflected by Mirror 3 and will pass through the receiver's filter. The signal is then focused onto the detector by the focusing lens.

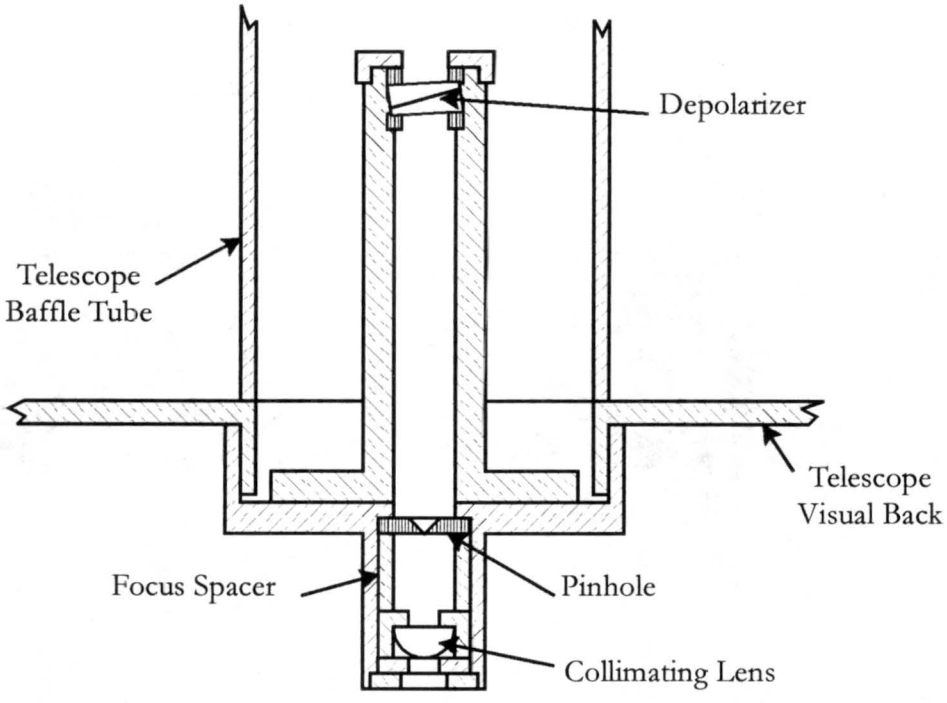

Figure 3.2 - Collimating lens, pinhole, depolarizer assembly.

3.2 OTA CONSTRUCTION AND ALIGNMENT

Alignment of the MPL optical train is tedious, but critical. The correct operation of the receiver demands that the transmitter (including shared optics) be properly aligned to minimize stray light. This section will discuss the elements of the construction and alignment in enough detail to inform the reader of the important points.

Most of the optical components of the OTA are mounted on platforms that allow movement along at least one axis. The optical elements and positioning equipment are available as off-the-shelf components by various manufacturers. The enclosure, miscellaneous mounts, and adapters that required custom manufacturing were fabricated either by a local machine shop or by the author. NASA had provided CSU with a full vendor list and complete set of mechanical drawings to copy their design. However, some

modifications were necessary not only to facilitate the enhancements of the EMPL but to fine tune the placement of items that had changed at the vendor.

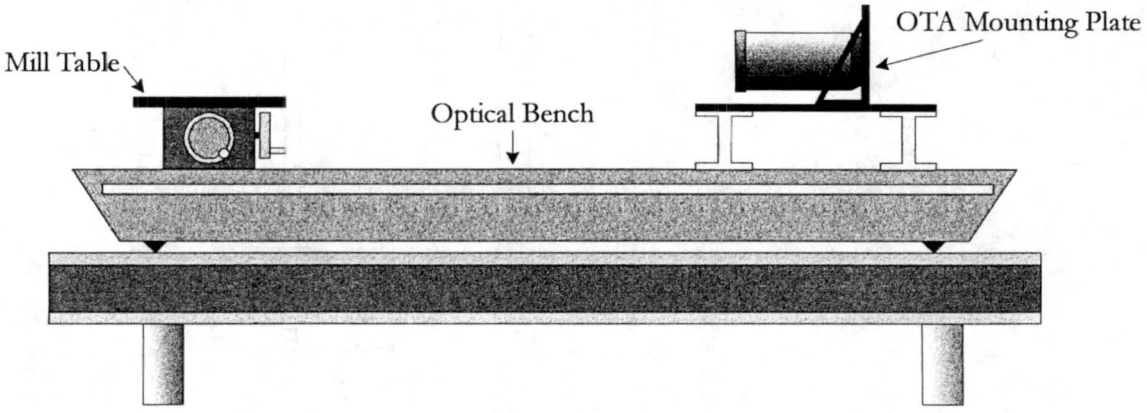

Figure 3.3 - The optical bench configuration.

A stable assembly platform in the form of a lathe table optical bench was used with two specially constructed platforms. The first platform was affixed to the optical bench at one end such that it was parallel to the axis of the bench. The second platform was installed on a milling machine table at the other end of the bench. The mill table can translate both parallel and perpendicular to the optical bench and can also rotate. The half-inch aluminum OTA mounting (top) plate was installed onto the fixed platform perpendicular to the platform surface such that when the telescope is installed it would be oriented parallel to the optical bench as illustrated in Figure 3.3. The optical bench not only provides a level, vibration resistant work surface but is long enough to mount alignment equipment on the movable platform at a sufficient distance from the OTA.

The telescope is mounted to the top plate from outside the OTA enclosure with the focusing knob and collimating lens housing passing through to the inside. Before installing any other component, the telescope is temporarily mounted such that the lens housing is centered in its opening in the top plate. Since, during the alignment procedure, the

telescope will be removed and installed several times, the location of the telescope is ensured by the installation of registration pins. During the first OTA assembly, holes were drilled through the telescope mounting brackets and into, but not through, the mounting plate while the telescope was securely fastened in the proper position. The telescope was then removed and registration pins pushed into the top plate. The holes through the brackets were re-drilled to prevent them from binding.

The first component to be installed on the inside of the OTA mounting plate is the laser. The laser head of the 2-watt[4] laser of the EMPL is substantially longer than the 1-watt versions of earlier MPL models and could not be installed in the location for which it was originally designed. The laser head was moved to the extreme edge of the mounting plate such that the rear of the laser head protrudes through the OTA enclosure. This design change accomplishes the relocation of the laser head and allows access to the RF and optical connectors from outside the enclosure. The laser head mount, OTA top plate, and enclosure side were modified to accommodate the change.

Once the laser is installed and its mounting hardware modified[5] to ensure that it is parallel to the top plate surface and top plate side, it is used as the light source to align the rest of the optics. The half-wave plate is then placed so that the laser beam is centered in and normal to the optic.

The next component to be installed in the optical train is Mirror 1. The mirror is attached to the mounting plate at a 45° angle with respect to the side of the plate. A plumb bob is hung from the lab ceiling such that the string hangs parallel to and the correct distance from the top plate. The plumb bob is positioned so that it also centered in the

---

[4] The power referred to here is the optical pump power.

[5] These modifications include elongating mounting hardware holes, shimming mounts, removing material from a mount, machining spacers, etc.

face of the mirror. The mirror mount is then adjusted until the laser light shines on the plumb bob string all the way to the ceiling. The location of the plumb bob is marked on the ceiling for future reference and the plumb bob is removed. This procedure guarantees that the beam is reflecting from the mirror orthogonally.

As suggested by the OTA physical layout figure, the retaining rings for Mirrors 1 and 2 had to be modified to accommodate the beam expander; the next item to be installed. As previously discussed, the beam expander is used to aid in beam collimation and it is also stopped down at its exit aperture to prevent light which is not in the main portion of the beam from propagating. The stop size and beam expansion factor were originally chosen to reduce the beam diameter to within the diffraction limit of a plano-convex singlet collimating lens. The appropriate stop size was calculated to be 2.5 mm. However, the singlet exhibited excessive blur and too much light was reflecting from the side of the pinhole. When it was replaced with an achromatic doublet, the stop was opened up to 4 mm. This size was somewhat arbitrarily chosen to allow more light to pass through the transmitter but to remain within the specified clear aperture of the beamsplitter cube. The beam expander position is adjusted by means of its mount so that the beam enters the device in the center of the entrance lens and leaves centered in the exit lens. When properly aligned, the area of maximum intensity of the beam will be located at the plumb bob mark on the ceiling of the lab. The aperture stop is then installed onto the beam expander.

Once the beam expander has been properly positioned, Mirror 2 can be installed. The mirror is attached to the mounting plate at a 45° angle and is properly adjusted when the reflected beam is parallel to both the top plate edge and its surface.

The beamsplitter positioning system consists of a mounting plate, a single axis translation stage, and an adjustable prism mount. The prism mount is new to the EMPL

and offers three degrees of freedom in the orientation of the polarizing cube. The entire assembly is attached to the mounting plate through slotted holes and is positioned by hand until the laser beam is centered in the cube face and the translation stage is square with the top plate. Once the beamsplitter assembly is securely fastened to the top plate, the prism mount is adjusted so that the beam is normally incident on the cube face. Then, the half-wave plate can be rotated so that the intensity of the beam passing straight through the cube is at a minimum. This guarantees that the maximum amount of energy is being reflected at the cube interface and is easily evaluated with a laser power meter.

The turning mirror positioning assembly consists of a single-axis translation stage and a 45° mirror mount. The translation stage is attached square to the OTA top plate and the mirror mount is then attached to it.

The next task, locating the focused transmitter beam through the pinhole, is probably the most difficult in the alignment procedure. If sufficient care is not taken, enough energy is concentrated by the collimating lens to burn through the edge of the pinhole. Also, if the focus is not correct or the orientation of the beam is such as to intensify spherical aberrations, enough light can be reflected from the edge of the pinhole back into the receiver to render the detector inoperable. Since the focus of the lens is measured with a microscope and then fixed by a spacer between the pinhole and the lens, only the orientation of the beam is adjusted.

To ensure that the focused beam is centered in the pinhole, the pinhole must be sighted from the telescope side of the top plate with an alignment telescope. This is only possible if the corrector plate and secondary mirror are removed from the telescope aperture. The depolarizer optic should also be removed. To avoid having to recollimate the telescope, the location and orientation of the corrector plate should be carefully noted.

Once the corrector plate has been removed, the location of the focused spot can be roughly positioned by sighting the pinhole through the receiver side of the beamsplitter cube. If the spot is not in the pinhole, it will be visible on the pinhole body. The spot can be moved by laterally displacing the beamsplitter cube and/or the turning mirror and by adjusting the turning mirror mount. Once the spot is in the pinhole, the centering adjustment can be made by observing the spot through the alignment telescope while manipulating only the turning mirror mount.

The depolarizer can now be reinstalled. It is mounted at a slight angle to prevent reflections from entering the receiver. The depolarizer functions best when its transmission axis is oriented 45° to the polarization state of the incident light (Temer, 1997). This can be observed by means of a polarizing element (e.g. a sheet polarizer) oriented such that its transmission axis is parallel to that of the laser light (i.e. the laser light passes unimpeded through the element). When the sheet polarizer is held at the output of the depolarizer and the processed light illuminates a screen, one can observe interference bands. The entire lens-pinhole-depolarizer assembly is then rotated until the bands are at a 45° angle with respect to the mounting plate. This is also when the bands are most pronounced. The lens-pinhole-depolarizer assembly can be locked into place by removing the telescope from the top plate and tightening the set screw of the assembly against the telescope visual back.

After the telescope has been reattached to the OTA mounting plate, the corrector plate and secondary mirror can be reinstalled in their previous orientation. The telescope can now be focused at infinity which requires a collimated source of light. To do this a hollow body retroreflector is used. This device has the property that all rays of light at its entrance aperture return offset but nearly perfectly parallel to the direction of entry. By mounting the retroreflector on the movable platform at the opposite end of the optical

bench and aligning it to be on axis with the telescope, transmit pulses can be used to focus at infinity. The telescope focus is adjusted until an image of the retroreflector is visible on the ceiling of the lab, which occurs when the rays leaving the telescope aperture are collimated.

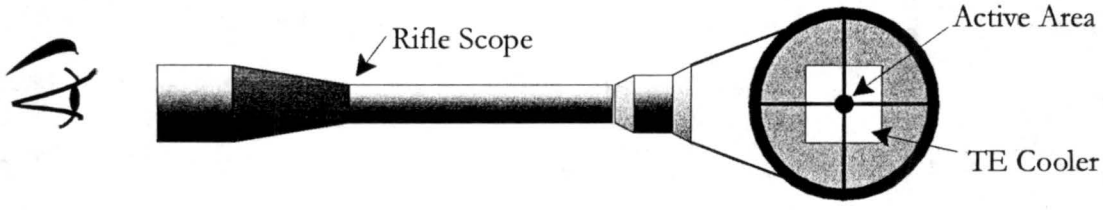

Figure 3.4 - Viewing the detector through an inverted rifle scope.

Once the telescope has been focused, Mirror 3 can be installed and adjusted until the beam is once again parallel with the mounting plate. Then, with the filter removed, the filter housing is installed and the focusing lens mount is attached to it. The assembly is moved by hand until the incoming rays are centered in the focusing lens. With the filter housing firmly secured to the mounting plate, the OTA telescope is removed and the entire assembly is affixed to the assembly platform so that the telescope side of the OTA mounting plate is facing down. The plate should also be rotated so that the detector line of sight is on axis with the optical bench. This is to position the detector for a new alignment procedure developed for the EMPL. Previously, the receiver was aligned by moving the detector while monitoring the background signal of a bright cloud (Spinhirne, 1993). The new procedure involves physically looking at the detector to determine its position and focus. However, the magnification of the aspheric focusing lens is infinite (Corning, 1993). To determine whether the detector plane is in focus and where the spot lies on the active area would require an observer to be located an infinite distance away. Although this cannot

not be physically done, it can be simulated by viewing the lens through an inverted rifle scope as illustrated in Figure 3.4. Assuming the telescope to be afocal, one can observe where a light ray would terminate on the detector by moving the observation point in the field of view of the inverted telescope. Consider the configuration of Figure 3.5(a). With the detector plane out of focus (in this case being too close to the lens), the observer would note that the crosshairs of the rifle scope would be located over different points on the detector when looking through the top edge as when sighting through the bottom edge of the scope. A similar condition would exist if the detector was too far from the lens as in Figure 3.5(c). It is only when the detector is centered and at the focal plane of the lens that the crosshairs of the scope remain centered over the active area regardless of the observation point. This is the target condition of the new detector alignment procedure.

The procedure begins by mounting the detector module and its three-axis translation stage to the OTA top plate. Then, Mirrors 2 and 3 are removed[6] to allow a direct line of sight through the focusing lens. The rifle scope is positioned to sight directly through the focusing lens. The translation stage is manipulated until the crosshairs are centered on the active area of the detector. The focus is adjusted until the crosshairs remain centered on the active area when viewed from all different positions in the rifle scope field of view.

After the detector has been aligned, the OTA mounting plate can be mounted perpendicularly as before. The telescope is then reinstalled and its focus readjusted. Mirrors 2 and 3 are then reinstalled and their orientation verified as before. Once it has been determined that the return beam is centered in the focusing lens, Mirror 3 can be removed and the filter installed. The filter is equipped with a polarizer and should be

[6] The mirrors should be fixed with registration pins to assure a repeatable orientation when reinstalled.

rotated to match the receiver's polarization sense. The mirror can then be replaced and the enclosure assembled. The OTA is then ready to be tested.

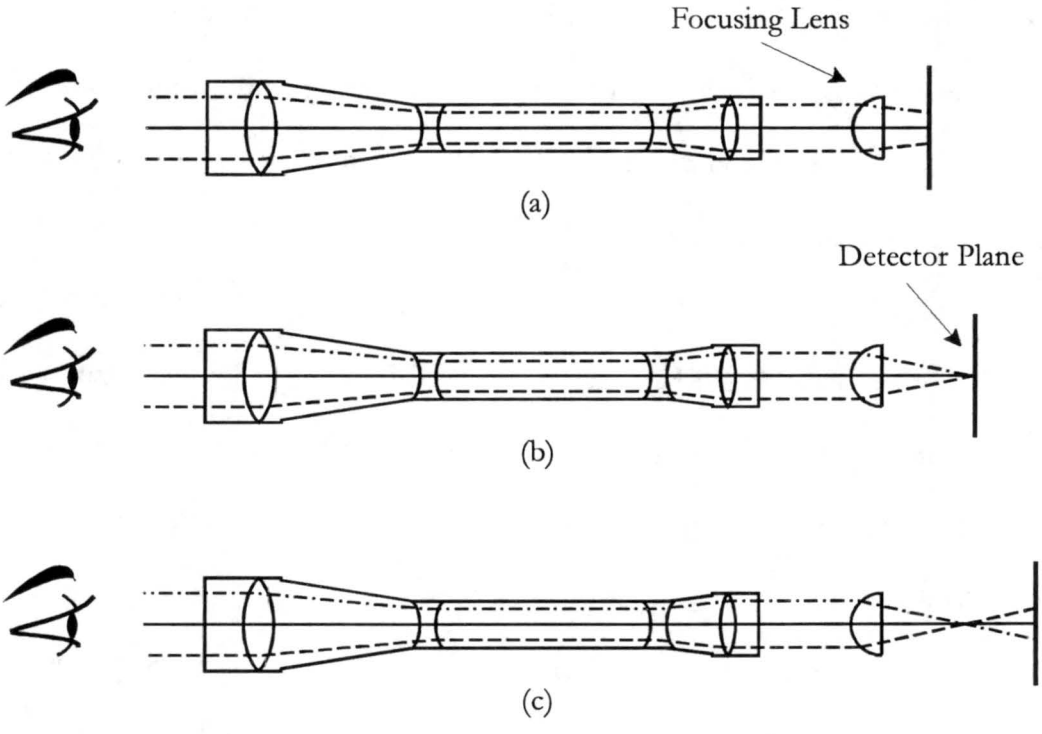

Figure 3.5 - Determining detector focus and position.

3.3 SYSTEM TESTING

As of the time this document was written, only the most fundamental form of testing had been performed on the EMPL system, i.e. the subjective inspection of varied data. To the first order, this form of testing has served well. The first several times the system was assembled and tested, it was obvious from the data that the system was performing poorly. Without exception, the symptom was the erroneously elevated count rate discussed earlier. The OTA had to be disassembled and components either replaced or repaired. Then, after the OTA had been reassembled, the system was tested again. The

process has been repeated several times until recently when the data appeared to match atmospheric conditions.

The main reason why more extensive testing of the EMPL has not been performed is the lack of a local standard for data comparison. That is to say, a simultaneous, collocated data acquisition undertaking with a similar, but calibrated device has not yet been coordinated. The EMPL was operating at the Department of Energy's Atmospheric Radiation Measurement (ARM) Cloud And Radiation Test bed (CART) site during the June, 1996 Cloud Layer Experiment (CLEX). A standard MPL is one of two lidars located at the ARM CART site. It was determined, however, that the EMPL was not performing satisfactorily so no data comparisons were made. Also, during the experiment, the detector was damaged which caused a lengthy delay before the system could be reassembled.

Figure 3.6(a) displays data from a layered cloud system which was witnessed by the author and others. The data portrayed in Figure 3.6(b) exhibit a strong return from an upper level cloud. Figures 3.6(c) and (d) illustrate some limiting cases; weak returns from high cirrus clouds. It is hoped that a new data filter, the implementation of which is planned for the future, will accent the features of the cloud in the signal more prominently. These four examples represent successful EMPL data acquisition the presence of clouds.

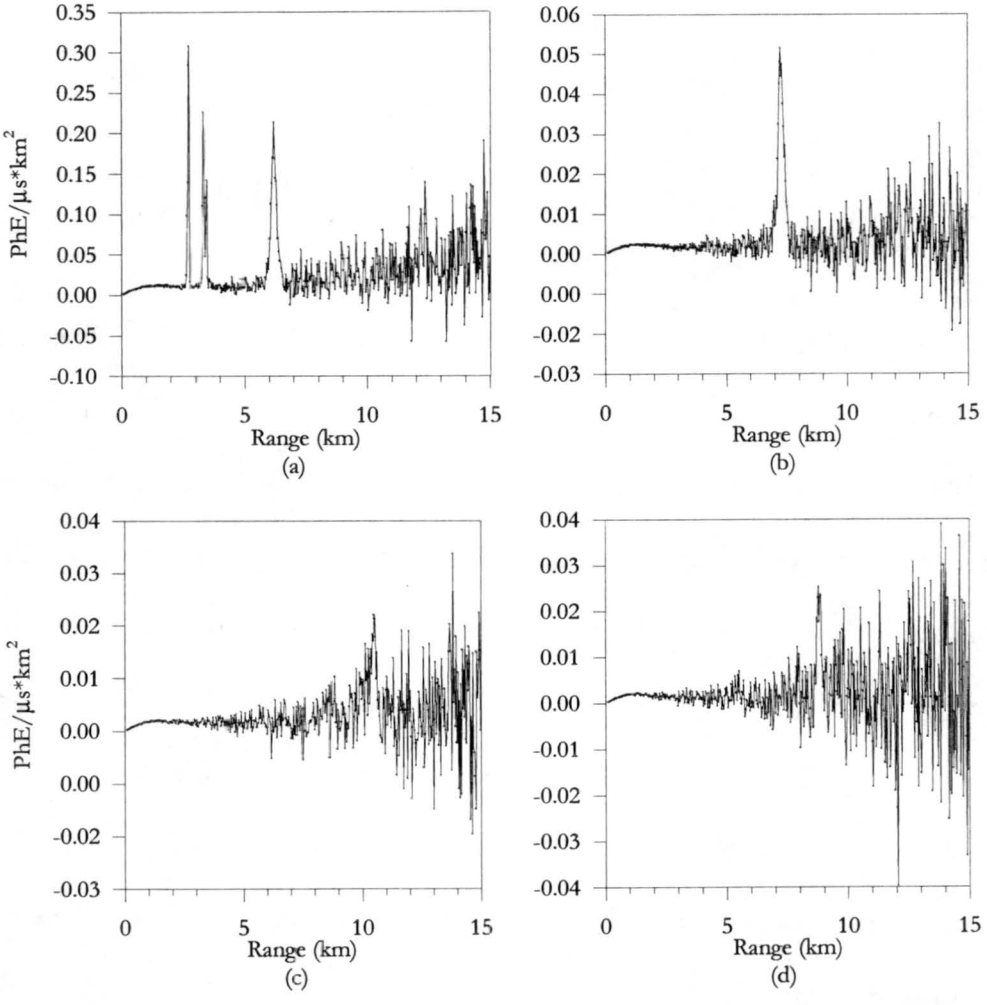

Figure 3.6 - Examples of typical EMPL data.

Chapter 4

SYSTEM TIMING AND CONTROL

The most significant difference between the EMPL and previous models is the addition of a user programmable timing and control system. The system allows the operator to adjust parameters in order to optimize the EMPL based on the phenomenon being studied. For example, consider the data presented in Figure 4.1 which presents a backscatter profile from a double-layered cloud system with a range resolution of 7.5 meters. Note that the entire double-peaked structure would fit into a single 300 meter range gate of the standard MPL. To acquire these data, the MCS of the EMPL was programmed with a 50 ns channel width. To accommodate the previously discussed end-of-pass deadtime for such a short range bin, the operating PRF had to be reduced to 1.7 kHz. Furthermore, since the clouds were located at a low altitude and were optically thick enough to discourage hope of obtaining meaningful data above them, only the low altitude data were archived. The retention of the data of higher altitudes would only consume valuable system memory without providing any useful information. This example illustrates a case where the researcher may wish to override the default system parameters used in the routine, unattended data-gathering mode of the EMPL to acquire details of a specific scenario. The operating parameters of the EMPL are easily adjusted via the system software which is the subject of the next chapter. This chapter will discuss the design and implementation of the timing and control system.

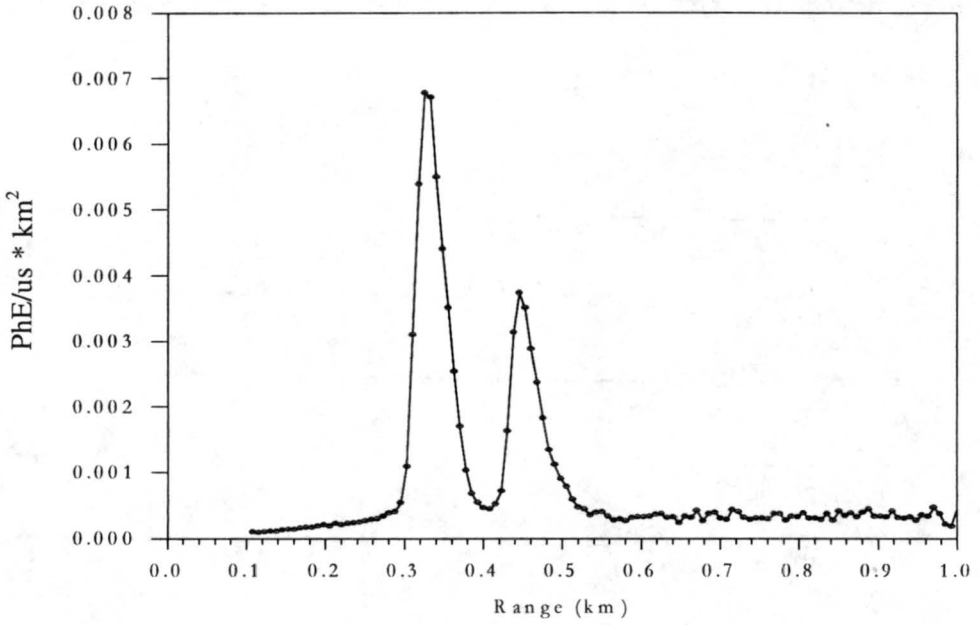

Figure 4.1 - The backscatter profile from a double-layered cloud system at 7.5 m resolution.

4.1 TIMING REQUIREMENTS

The timing system controls the pulse repetition frequency as well as coordinating the necessary delays for system synchronization. Referring now to the timing diagram of Figure 4.2, the timing cycle begins every t_{PRP} with the rising edge of XMIT (transmit). This causes the removal of the RF signal from the laser head's Q-switch. The rising edge of XMIT also triggers Q2P (Q-switch to pulse) which is a delay to compensate for the laser pulse formation time. After the specified delay time, t_{Q2P}, the rising edge of Q2P triggers !BLANK, an active TTL low which activates the detector blanking circuit. The timing periods t_{Q2P} and t_{BLNK} are adjusted so that the detector is disabled while the laser pulse is traversing the EMPL transmitter circuit. The !BLANK signal is introduced to the input of a delay line which retards the pulse by t_{B2A}. The newly created signal, ACQ (acquire), is used to trigger the MCS to begin data collection. The delay is used to allow the system to settle

from fluorescence, after-pulsing, etc. before the data collection scan begins. At present the timing signals are observed on an oscilloscope and adjusted as necessary. However, a look-up table with appropriate values of t_{Q2P}, t_{BLNK}, and t_{B2A} as functions of optical pump power and PRF is planned for the future.

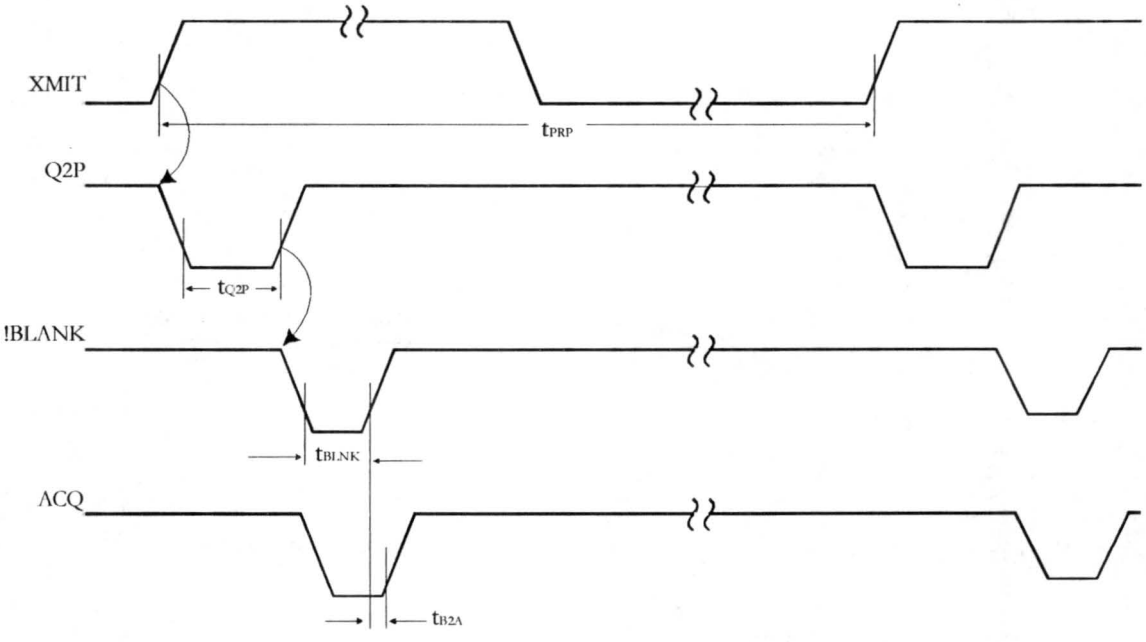

Figure 4.2 - EMPL timing waveforms.

There is a further timing requirement for the MCS. When the instrument is being externally triggered, the data stream must be delayed 30 ns in order to count correctly into the first range bin. Since the output impedance of the OTA detector and the input impedance of the MCS are both 50 ohms, the specified delay was introduced by a length of RG-58 coaxial cable. Knowing the velocity factor of the cable to be 0.66, a 30 ns delay requires 6 meters length. The cable was manufactured and inserted between the detector and MCS.

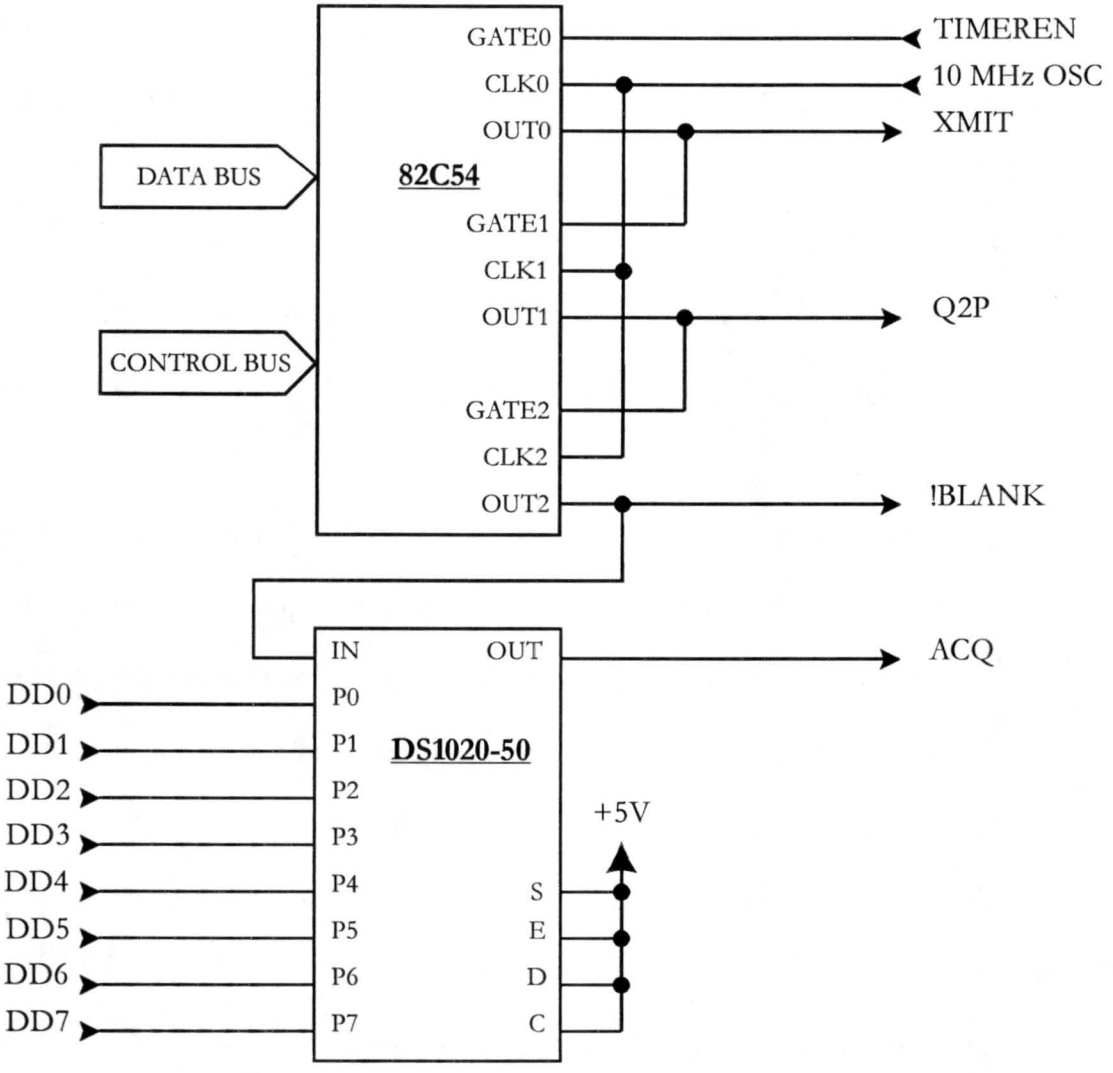

Figure 4.3 - The EMPL system timer.

4.2 TIMING IMPLEMENTATION

At the heart of the system timer is the Intel 82C54 Programmable Interval Timer (PIT) which is located on an off-the-shelf timer and digital I/O board, Omega Engineering's CIO-DIO24/CTR3. A schematic diagram of the timing implementation is given in Figure 4.3. The PIT consists of three 16 bit counters which are independently programmable. Counter 0 divides the 10 MHz master oscillator (which is also located on the CIO-DIO24/CTR3) to realize the pulse repetition frequency at a 50% duty cycle. The

control signal, TIMEREN enables and disables Counter 0. TIMEREN is issued by software command and is generated by another chip on the CIO-DIO24/CTR3, an Intel 82C55 programmable peripheral interface (PPI). The implementation of TIMEREN and other control signals is discussed below.

Counter 1 is configured as a hardware retriggerable one-shot. OUT1 is initially high and remains so until a rising edge is presented to GATE1. As is evident in the schematic, the trigger is supplied by OUT0 otherwise known as XMIT. The output of Counter 1 changes state and remains at TTL low until the programmed count value has elapsed. The result is the signal Q2P on OUT1. Counter 2 is configured just as Counter 1 is (except for possibly a different count value) and produces !BLANK when triggered by Q2P.

The output of Counter 2, i.e. !BLANK, is supplied to the input of a Dallas Semiconductor DS1020-50 programmable 8-bit silicon delay line which is located in the Distribution Panel. The chip can delay the input pulse from 10.0 ns to 137.5 ns in 0.5 ns increments. The delay time is programmed via a binary value set on pins P0-P7. The delay data lines DD0-DD7 are under software control via the PPI. The pins S, E, D, and C are kept at TTL high and are not important to this discussion. The resulting waveform at the output of the chip is ACQ.

Data acquisition requires synchronization, but before the data collection cycle is discussed, we first must define some terms. The highest order fundamental unit of EMPL data is the *frame*. Each frame consists of a user-specified number of integrated background and backscatter *sets*. A single data collection cycle be it for background or backscatter data is referred to as a *scan*. At the beginning of a frame, a background measurement is made by collecting data without firing the laser. After a user-specified number of seconds, a new scan is started, this time with the laser enabled to collect backscatter data. This is the first

set of the data frame. As new scans are done, new background data are co-added with those previously collected. The same process is applied to the backscatter data. The number of sets per frame is determined by the EMPL user.

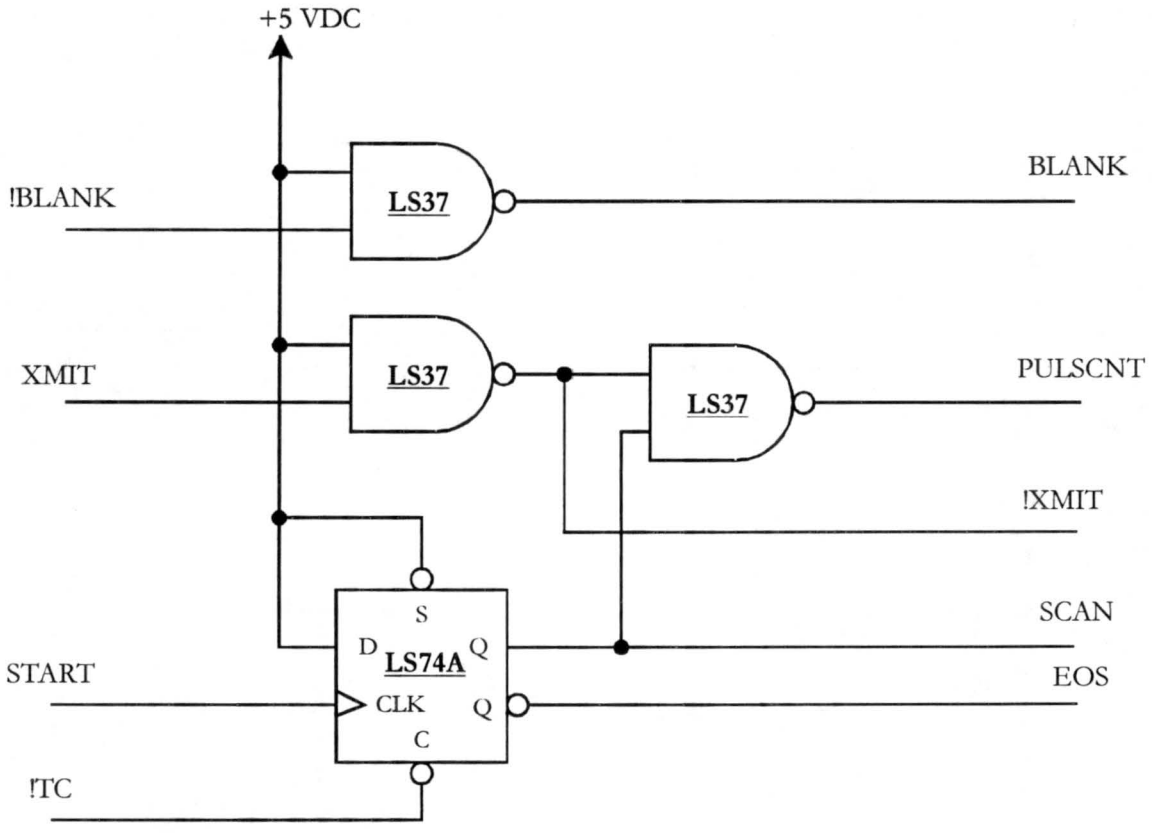

Figure 4.4 - Data acquisition control.

The circuitry to implement the timing control, which is housed in the DP, is depicted in Figure 4.4. At the beginning of a frame, !TC (Terminal Count, an active low signal from the 32-bit pulse counter) is set high and the system timer enabled. At the appropriate time, the software issues a START pulse which sets SCAN high. This allows not only XMIT, !BLANK, and ACQ to propagate through the 74S140 50 ohm line drivers (as is illustrated in Figure 4.5), but also sends PULSCNT to the pulse counter. Note that the order in which a frame's data are acquired is background first and then backscatter so

when the frame starts, XEN is low which inhibits firing of the laser. When the pulse counter counts down to zero, !TC goes low which accomplishes two things. First, SCAN goes low and the 50 ohm line drivers are then blocked. Also, EOS goes high and, as it is tied to an IRQ line of the PC, initiates an interrupt. The interrupt service routine, which is discussed in the next chapter, prepares the system for the next scan.

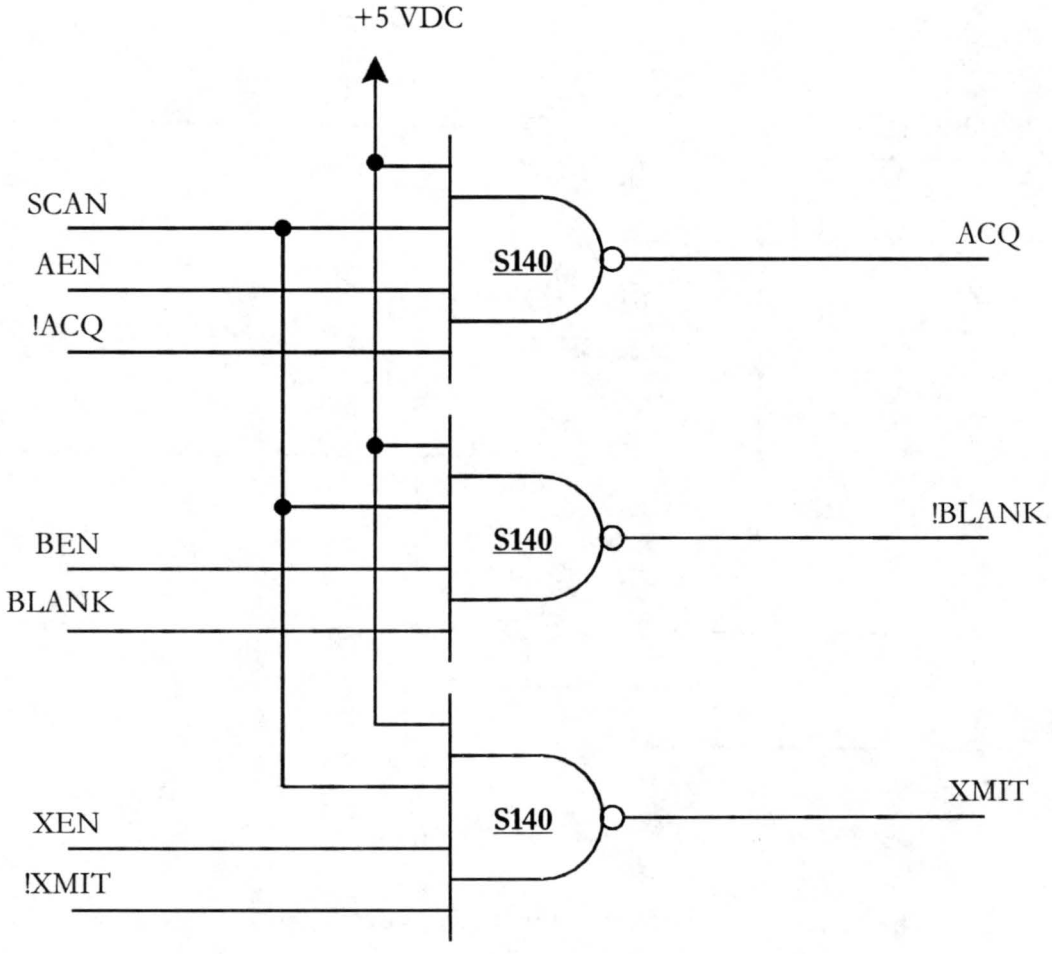

Figure 4.5 - Timing output control.

4.3 SYSTEM MONITORING AND CONTROL

All of the EMPL subsystems require at least minimal control and most require monitoring of vital functions. It was desired that the PC be the universal interface to all

subsystems and, to save on design time, the system is made up of as many off-the-shelf items as were available. Omega Engineering's CIO-DIO24/CTR3 board provides main timing functions and digital control lines. To monitor analog signals, Analog Device's RTI-815A A/D Digital I/O board was chosen primarily because unused units were already available within the Department of Atmospheric Science. The RTI-815A employs an Advanced Micro Devices Am9513A System Timing Controller on board which is used for pulse counting.

The MCS is the most self-supporting unit requiring only communication through a manufacturer supplied interface card. Through the interface card, diagnostics, unit configuration and data collection can all be performed under software control.

There are many functions of the OTA which require either monitoring or control. First is the 0.8 Angstrom etalon filter that is situated just before the detector focusing lens in the receiver path. Because the filter's passband is so narrow and the spacing of the etalon elements can change with temperature, the optical element is mounted in a temperature regulated oven. As delivered, the oven is equipped with a thermistor for temperature monitoring and a bimetallic switch for temperature control. However, the bimetallic switches have been known to fail and so a more reliable temperature control method was instituted. The thermistor was removed and a resistive thermal device (RTD) installed in its place. The RTD is used as a feedback element in a proportional-integral-derivative (PID) control system using Omega Engineering's CN76000 Microprocessor-based temperature controller (TC). The filter temperature was adjusted so that maximum transmission through the filter (at 523.5 nm) was achieved. It was found that at 48° C, the maximum transmission of the filter was 19.27% . The filter temperature regulator circuit is given in Figure 4.6. Note the use of a solid state relay (SSR) to handle the load of the filter's heater.

The OTA enclosure temperature and detector case temperature are monitored by simple thermistor voltage divider networks into the A/D card. The detector can dissipate a relatively large amount of heat during high count rates and its temperature should not be allowed to exceed 30° C for any length of time

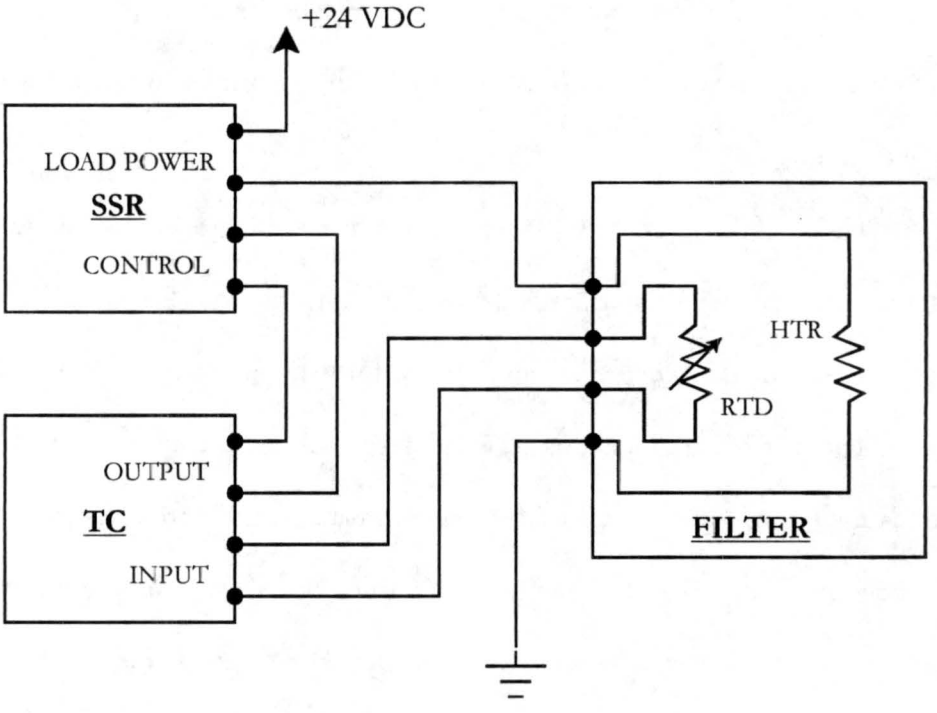

Figure 4.6 - The etalon filter temperature control circuit.

The laser system's functions are completely accessible through a connector on the LDM. Optical pump diode temperatures and current flow is monitored by the A/D - D/A card. The optical pump power is controlled by the D/A section of the RTI-815A. Also present on the RTI-815A is an AMD Am9513A system timer which has three 16-bit timers that are not being used by the board. Two of these timers are cascaded to produce a 32-bit counter which is used to keep track of transmit pulses.

The digital control lines of the laser, as well as other sub-systems, are manipulated by the PPI on the CIO-DIO24/CTR3 board. The PPI is configured in this application as

one 8-bit input port, one 8-bit output port and a port of 8 single bit set/reset lines. The PPI is illustrated in Figure 4.7 and the various signals are detailed in the table below. The orchestra comprised of the control elements of the EMPL are conducted by the system software which is the subject of the next chapter.

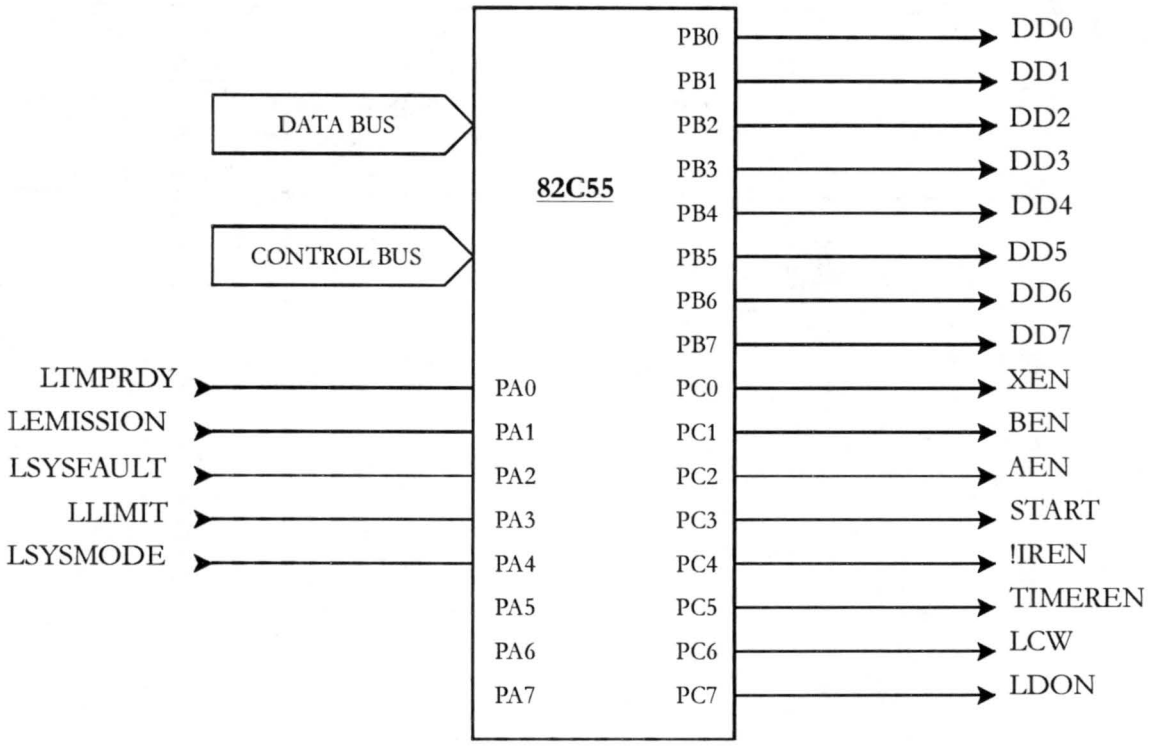

Figure 4.7 - The EMPL digital controller.

Table 4.1 - 82C55 Port Assignments

SIGNAL NAME	FULL NAME	DESCRIPTION
DD0 - DD7	Delay Line Data	Controls the amount of delay on the ACQ delay line.
XEN	Transmit Enable	Allows trigger pulses (XMIT) to be sent to the LDM.
BEN	Blank Enable	Allows blank pulses (!BLANK) to be sent to the detector.
AEN	Acquire Enable	Allows trigger pulses (ACQ) to be sent to the MCS.
START	Start	Initiates a data collection scan.
!IREN	Interrupt Enable	Allows the IRQ line to be used for end of scan (EOS) interrupt.

SIGNAL NAME	FULL NAME	DESCRIPTION
TIMEREN	Timer Enable	Activates the system timer.
LCW	Laser Continuos Wave	Puts the laser in continuos wave (CW) mode or pulsed mode.
LDON	Laser diode on	Activates optical pump diode emissions.
LTMPRDY	Laser temperature ready	Reports that laser temperature is stabilized.
LEMISSION	Laser emission	Reports that optical pump diodes are emitting.
LSYSFAULT	Laser system fault	Reports a laser system fault.
LLIMIT	Laser limit	Reports that optical pump diode cannot attain a power or current setting.
LSYSMODE	Laser system mode	Reports that the LDM is being controlled through the user interface as opposed to the remote control.

Chapter 5

SYSTEM SOFTWARE

Much of the time necessary to develop the EMPL to this point has been devoted to system software. The program provides system control and monitoring as well as user interface, data archival and real-time data display. The details of the system software are somewhat complex so this chapter will describe only the main components. A detailed software users manual is planned for the future.

5.1 USER INTERFACE AND DISPLAY

With few exceptions, the EMPL data display has the look and feel of the MPL display. The display screen is divided into several panels as is exhibited in the photograph in Appendix F. The two large panels are used to display processed data. The upper section displays the latest backscatter profile and the lower panel displays a long term, color-coded return intensity plot. The lower section along the right side of the screen is the background level plot which is used to display the strength of the background signal. This portion of the display has not been fully implemented primarily due to future decisions regarding signal processing which need to be made. Above the background plot is the system status panel which displays various component temperatures, timing parameters, indicators of whether the backscatter data are range-corrected, overlap-corrected, and are being displayed in a log or linear scale. Immediately above the status panel is the time inset which displays the current time as well as that of the acquisition time of the current frame.

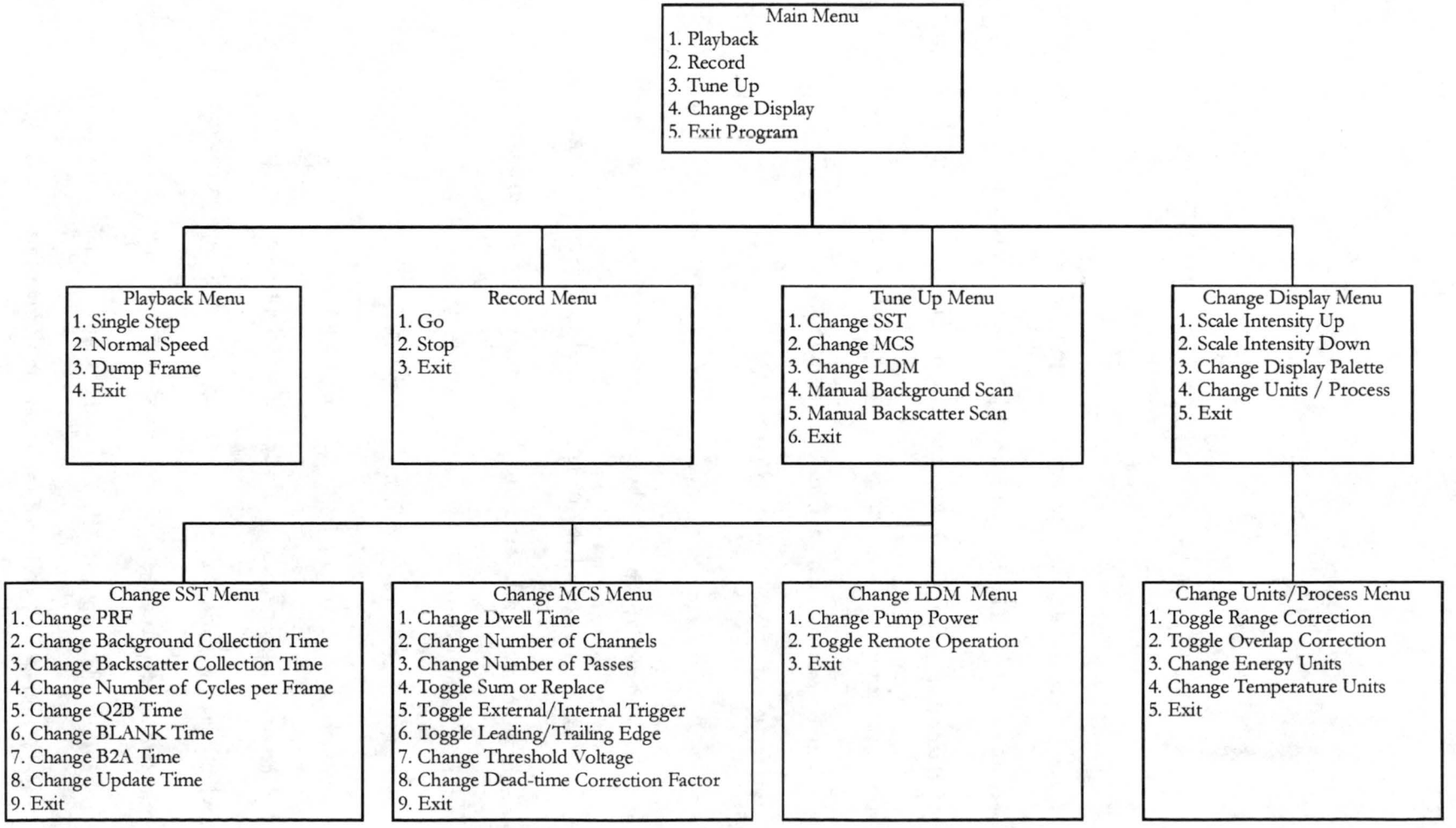

Figure 5.1 - Software menu structure.

The inset in the upper right corner of the display is the menu panel through which the bulk of user interaction occurs. The menus are arranged in a top-down architecture, i.e. from a upper-level menu either an action or sub-menu can be selected and leaving a sub-menu reverts control to the menu above it. The basic menu layout is depicted in Figure 5.1. The main menu is the top-most menu and is displayed upon execution of the program. From it the Playback, Record, Tune Up, and Change Display sub-menus can be chosen. The Playback menu offers a manual or automatic frame viewing mode as well as the capability to dump a frame's data into an ASCII file (a sample of such a file is given in Appendix C). The Record menu controls the starting and stopping of data acquisition which is explained in the next section. From the Tune Up menu, the user can select sub-menus to change the operating parameters of the System Synchronizer-Timer (SST), the MCS, and the LDM as well as perform a single background or backscatter scan for performance testing. The Change Display menu gives options to scale the level of the color-coded intensity plot, change the color palette of the display, and to choose the sub-menu that controls various display units and data correction algorithms. The options offered by the sub-menus under the Tune Up and Change Display menus are self-explanatory and their purpose can easily be derived from the diagram.

All of the EMPL parameters are stored as ASCII text in the initialization file, MPLSYS.INI, and can be manipulated through the use of any text editor. The file is read upon execution of the main program, MPLCSU.EXE, and from it the system variables are initialized. System parameters that are changed through a menu selection are automatically stored in the initialization file. A typical configuration is given in Appendix C.

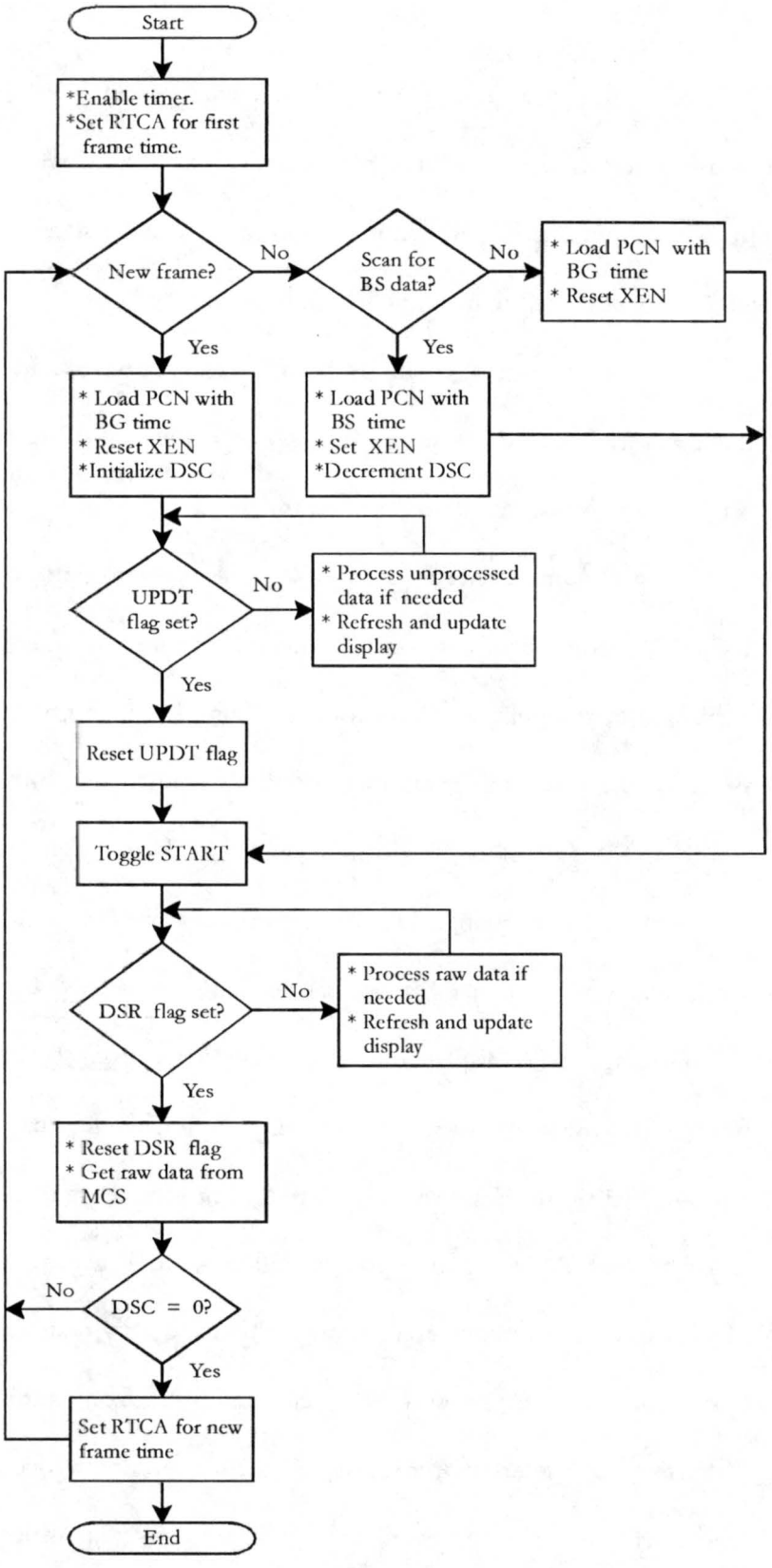

Figure 5.2 - Data acquisition flowchart.

5.2 DATA ACQUISITION

As previously explained, data are collected in a series of sets. First, background data are taken for a user-specified length of time and then backscatter data are taken. It is important that the measurement period for an individual data set be short enough that the background signal for both scans can be considered constant. This can be a problem when broken clouds moving with the wind traverse the transceiver's narrow field of view. Furthermore, the summation of several series of correlated data improves the signal-to-noise ratio. Both of these concerns are addressed by summing several sets which, individually, are collected over a short period of time. The number of data sets to integrate, the time to collect background data, and the time to collect backscatter data are all individually set by the user.

In order to process and display data in real time, the data acquisition cycle is primarily interrupt driven. First, an interrupt service routine (ISR) is placed at the PC's real-time clock alarm (RTCA) interrupt vector location 4A (hex). The alarm is set to the desired time for the start of a new frame. When the alarm goes off, the ISR sets a variable called the Update (UPDT) flag. The software regularly polls the flag and when set, begins the data taking cycle.

The other interrupt used is an Interrupt Request (IRQ) line to signal the system that data are ready to be transferred from the MCS to the PC. The IRQ ISR is called when the 32-bit transmit pulse counter (PCN) reaches its terminal count. The ISR sets the Data Set Ready (DSR) flag which is also polled by the software and raw data are then retrieved from the MCS.

The basic data collection cycle is depicted in Figure 5.2. When the system starts to record data, the system timer is enabled (TIMEREN set high) and the RTC alarm is

initialized with the first frame time. Then, the PCN is loaded with the desired number of background (BG) pulses and the Data Set Counter (DSC) is programmed with the desired number of set integrations. The control signal XEN is reset to prevent the laser from firing. The system can then perform processing and updating the display while continually polling the Update Flag. When the RTCA ISR sets the UPDT flag, the control signal START is toggled and the system begins to collect background data. At this point, the system can process data previously collected (if this is the first frame, of course there are none) or other chores while monitoring the DSR flag. When the PCN reaches zero count, the IRQ ISR will set the DSR flag and data can be retrieved from the MCS. Since the DSC is not decremented until a complete data set has been acquired, the process is repeated except that now backscatter (BS) data are to be collected so the laser is enabled.

Processed data are displayed after each data set is collected. After the second set is acquired, its background data is added to the previous set's as is its backscatter data to the previous set's backscatter data. The newly created set is then reprocessed and redisplayed. This procedure is repeated until the DSC reaches zero and the frame is complete. The finished frame is then stored to disk in the format described in Appendix E.

5.3 SIGNAL PROCESSING

At present, only rudimentary signal processing is done and this portion of the research is still in development. In this section, we can discuss the nature of the signal, what type of processing has been done in previous MPL systems and what is being done in the EMPL.

There are several data processing steps in current and previous MPL models. First, the signal is compensated for detector deadtime and the background signal is removed from the backscatter signal. The signal can then be optionally overlap and/or range corrected.

These are the same steps used in the EMPL, however some of the procedures have not been fully implemented.

Consider the receiver's architecture. The incoming radiation is first polarized by the polarizing beamsplitter cube and the filter's polarizer is rotated to match. The filter has a very narrow bandwidth and is calibrated (by adjusting the oven temperature) to the laser wavelength of 523.5 nm. The light is then focused onto the very small active area of the detector so we can assume an even intensity distribution. Under these conditions, Helstrom (1995) defines a probability distribution for the output signal. The light incident on the detector can be represented by,

$$v(t) = \Re\left\{V(t)e^{j\Omega t}\right\}$$

where $V(t)$ is the radiation's complex envelope and Ω is its angular frequency. If the detector does not become saturated, then the conditional probability that a photoelectron will be countable is

$$\lambda(t)T = \frac{\eta'}{2hf}\left|V(t)\right|^2 T$$

where $\lambda(t)$ is the instantaneous rate of emission, η' is the detector quantum efficiency, h is Planck's constant 6.626×10^{-34} J·s, f is the frequency of the incident radiation, and T is the observation period from a t_1 to t_2. Then, the probability that the number of photoelectrons, n, in a given time interval will be equal to k is

$$P\left[n = k \middle| V(t), t_1 \le t \le t_2\right] = \frac{m^k}{k!}e^{-m}$$

where

$$m = \int_{t_1}^{t_2} \lambda(t)dt .$$

This, of course, is the well known Poisson distribution.

As previously discussed, not all photons will be counted due to the finite deadtime of the detector. If we assume that the instantaneous rate of emission is constant during the observation period T, i.e.

$$m = \lambda T$$

then the distribution function for a photocount from a detector with specified deadtime, τ, is not the Poisson but is given by (Cantor and Teich, 1975),

$$P\left[n = k \middle| \lambda, T, \tau\right] = \sum_{i=0}^{k} \frac{\lambda^i (T - k\tau)^i}{i!} e^{-\lambda(T-k\tau)} - \sum_{i=0}^{k-1} \frac{\lambda^i \left[T - (k-1)\tau\right]^i}{i!} e^{-\lambda\left[T-(k-1)\tau\right]}.$$

The mean and variance for this distribution are, respectively,

$$\overline{n} = \frac{\lambda T}{1+\lambda\tau} + \frac{1}{2}\left(\frac{\lambda\tau}{1+\lambda\tau}\right)^2$$

and

$$\sigma^2 = \frac{\lambda T}{(1+\lambda\tau)^3}.$$

Note that the mean and variance are not equivalent as in the pure Poissonian case (Walpole and Myers, 1989). However, when $\tau = 0$, the probability distribution function (PDF) given above reverts to that of the Poisson distribution and the mean and variance are both λT. For the PDF given above, the maximum likelihood (ML) estimator, $\hat{n}$, to $\overline{n}$, the average number of absorbed photons, is given by (Sun and Davidson, 1992),

$$\hat{n} = \frac{k}{1 - k\left(\frac{\tau}{T}\right)}$$

where k is the number of photons actually detected. For a non-zero deadtime, Sun and Davidson (1992) also show that the application of this estimator results in a non-zero

average estimation error and larger variance culminating in a lower signal-to-noise ratio (SNR). The extent to which this is true is dependent on the quotient (τ/T) and the count rate.

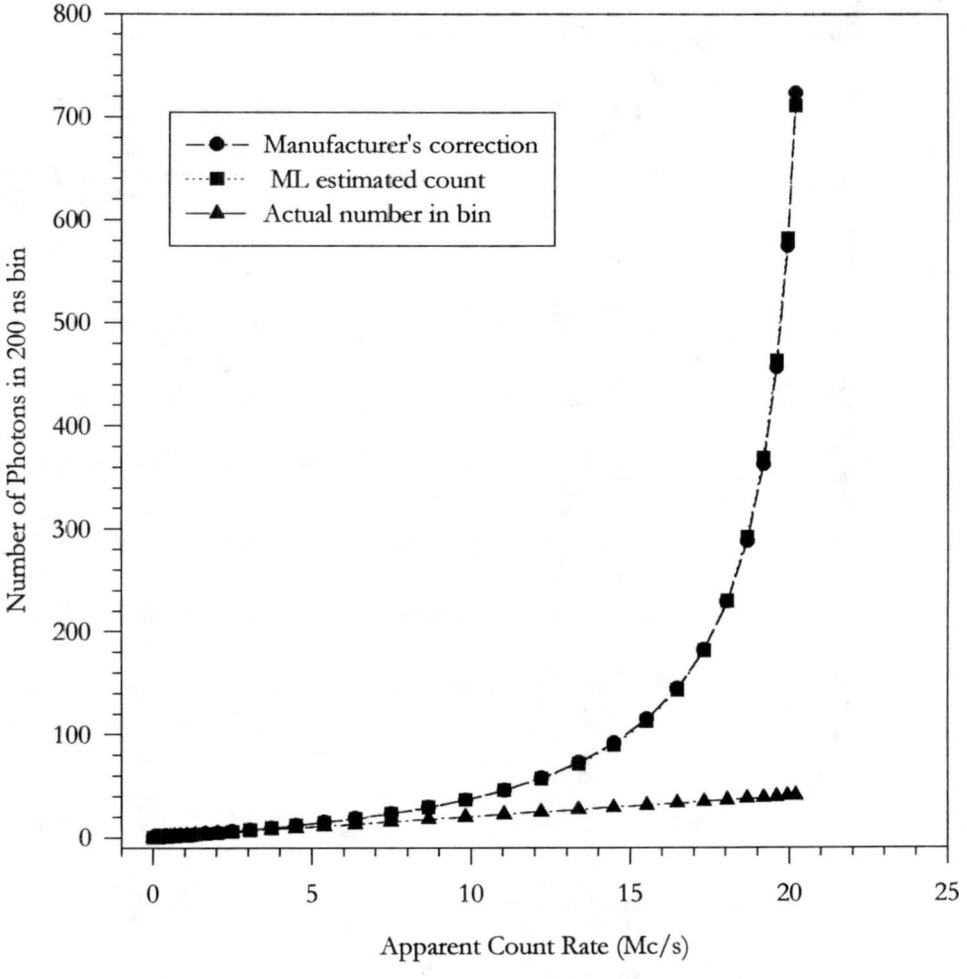

Figure 5.3 - ML estimator of deadtime correction factor.

Although the Department of Atmospheric Science does not have the means to measure the deadtime, τ, the detector manufacturer provides a deadtime correction curve. The data for this curve are supplied as a series of discrete deadtime correction factors as a function of a count rate. The manufacturer's data were used in a curve fit to find a value for τ (actually, the curve fitter was used to find τ/T for a given bin length). Figure 5.3 show these data for the case of T=200 ns where τ was found to be 46.68 ns. Note that, as expected, the greatest difference between the estimation and measured curves occur at the highest count rate. The utilization of the ML estimator is unique to the EMPL and will be studied further as the development of the instrument continues. Earlier MPL systems also adjust for detector deadtime, but a slower exponential curve fit corrector is used.

The next signal processing step is the removal of the background signal. There are two methods being used by MPL systems to obtain the background measurement. The first method uses a sub-series of data at the end of the backscatter data series. The assumption is made that no backscatter signal is available from targets at such a high altitude and the sub-series consists only of background. Most MPL models use this method. The EMPL, however, takes an independent background measurement while laser firings are inhibited. This method offers some advantages. First, the background signal is guaranteed to be uncontaminated by the laser signal which, other than the obvious benefit of assured signal purity, can aid in system diagnostics. If the count rate of the detector is elevated from an input overload as discussed earlier, it will be clearly evident in the data after background subtraction. Another advantage of an independent background measurement is a longer time series for determining the statistics of the background series. It is hoped that the information will be useful when a new data filter is implemented. As of this writing,

both MPL and EMPL determine a average background level and subtract it point by point from the backscatter series.

In Chapter 1, the transceiver geometric overlap was discussed. It is a necessary data adjustment that previous MPL models have hardwired into their software after the calibration data are taken by direct measurement. However, the length and number of range bins for the EMPL are user-programmable values. Therefore, the overlap coefficients cannot be hardwired into the code. For this reason, the application of overlap correction has not yet been implemented in the EMPL. One possible solution is to engage a routine based on the theoretical work done by Harms (1979). Another would be to make a direct measurement and curve-fit the results. The method of overlap correction is one of several future projects slated for the near future.

Chapter 6

CONCLUSIONS AND FUTURE WORK

6.1 CONCLUSIONS

This document has described the Enhanced Micro Pulse Lidar from first principles and detailed the improvements that were made to the original NASA design.

- The addition of the higher power laser will provide greater range coverage with only slight operating adjustments to maintain eye-safety be made.
- The new multichannel scaler has increased the range resolution of the device. The calculation time required for detector deadtime compensation has been improved by means of a maximum-likelihood estimator.
- A new alignment procedure that does not require expensive equipment has been developed and documented.
- A user-programmable timing and control system has been designed and implemented. Through the system software, the operator can easily adjust operating parameters such as pulse repetition frequency, detector blank time, number of data integrations and bin size to name just a few. The flexibility of the system makes it possible to optimize the performance of the EMPL for different meteorological applications.

6.2 FUTURE WORK

Some of the proposed future projects have already been discussed in previous chapters. Among them are the design and implementation of a transceiver geometric

overlap correction procedure. Also, a data filter that can extract the backscatter profile from the returned signal based on the statistics of the background measurement is desired. But many other activities are planned.

First, a decision as to the level of calibration has to be made. A high degree of calibration requires sophisticated equipment and procedures, but also provides more reliable data. Once the degree of accuracy has been determined, a procedure must be designed and executed. A thorough calibration of the instrument (i.e. determination of optical transmission efficiencies, detector quantum efficiency, range verification, etc.) may furnish insight as to how to improve performance.

The desire to study the depolarization of the transmitted beam by the atmosphere has also been discussed. This would involve transmitting pulses of alternating, orthogonal polarization states and measuring the returned light separately. Since most schemes to accomplish this require expensive modifications to the EMPL, it is unlikely that this project will be attempted in the near future.

The EMPL was designed to allow the user to ask "What would happen if I ...?". The ability to change operating parameters such as range bin size or PRF as conditions warrant can provide the researcher with a diverse data set. As experience with the instrument grows, so does the list of suggested improvements. Therefore, the EMPL will most assuredly continue to evolve throughout its useful lifetime.

REFERENCES

Advanced Micro Devices, 1990: **Am9513A/Am9513 System Timing Controller Technical Manual**, 115 pp.

ANSI (American National Standards Institute), 1993: **American National Standard for the Safe Use of Lasers, ANSI Z136.1-1993**, ANSI, 94 pp.

Analog Devices, Inc., 1986: **RTI-800/815 User's Manual**, Analog Devices, 110 pp.

Cantor, B. I. And M. C. Teich, 1975: Dead-time-corrected photocounting distributions for laser radiation. *J. Optical Society of America*, **65**, 786-791.

Carswell, A. I., 1983: Lidar measurements of the atmosphere. *Canadian J. Physics*, **61**, 378-395.

Celestron International, 1994: **Celestron 8 Instruction Manual**, Celestron International, 121 pp.

Collis, R. T. H. and P. B. Russell, 1976: Lidar measurement of particles and gases by elastic backscattering and differential absorption. *In* **Laser Monitoring of the Atmosphere**. E. D. Hinkley, Ed. Springer-Verlag, Chapter 4.

Corning, Inc., 1993: **Precision Molded Optics Glass Aspheric Lens Technologies**, Corning, Inc., 24 pp.

Cotturone, J. A. and S. K. Cox, 1996: **Monte Carlo Simulation of Detection of Cirrus Cloud Properties by Micro Pulse Lidar**, Colorado State University Department of Atmospheric Science Blue Book Paper Number 608, 58 pp.

Cova, S., A. Longoni, and G. Ripamonti, 1982: Active-quenching and gating circuits for single-photon avalanche diodes (SPADs). *IEEE Trans. Nuclear Science*, **NS-29**, 599-601.

CVI Laser Corp., Unknown: **Polarization Optics Guidebook**, CVI Laser Corp., 60 pp.

Dallas Semiconductor Corporation, 1994: **System Extension Data Book**, Dallas Semiconductor Corporation, 502 pp.

Dautet, H., P. Deschamps, B. Dion, A. D. MacGregor, D. MacSween, R. J. McIntyre, C. Trottier, and P. Webb, 1993: Photon counting techniques with silicone avalanche photodiodes. *Applied Optics*, **32**, 3894-3900.

Edde, B., 1993: **RADAR: Principles, Technology, Applications**, PTR Prentice-Hall, 717 pp.

EG&G Optoelectronics, 1994: **Single Photon Counting Module SPCM-AQ Series Provisional Data Sheet**, EG&G, 6 pp.

EG&G Optoelectronics, 1996: **Single Photon Counting Module SPCM-AQ Series Instruction Manual**, EG&G, 8 pp.

EG&G Princeton Applied Research, unknown: **Model 914P Multichannel Scaler Users Manual**, EG&G, 173 pp.

Harms, J., 1979: Lidar return signals for coaxial and noncoaxial systems with central obstructions. *Applied Optics*, **18**, 1559-1566.

Hecht, E., 1987: **Optics**, Addison-Wesley, 676 pp.

Helstrom, C. W., 1995: **Elements of Signal Detection and Estimation**, PTR Prentice-Hall, 586 pp.

Ingerson, T. E., R. J. Kearney, and R. L. Coulter, 1983: Photon counting with photodiodes. *Applied Optics*, **22**, 2013-2018.

Intel Corporation, 1985: **Microsystem Components Handbook, Volume II**, Intel Corporation, Chapter 5.

Jelalian, A. V., 1992: **Laser Radar Systems**, Artech House, 292pp.

Klett, J. D., 1981: Stable analytical inversion solution for processing lidar returns. *Applied Optics*, **20**, 211-220.

Kunz, G. J. and G. de Leeuw, 1991: Inversion of lidar signals with the slope method. *Applied Optics*, **32**, 3249-3256.

Lacaita, A., S. Cova, C. Samori, and M. Ghioni, 1995: Performance optimization of active quenching circuits for picosecond timing with single photon avalanche diodes. *Review of Scientific Instruments*, **66**, 4289-4295.

Liou, K., 1980: **An Introduction to Atmospheric Radiation**, Academic Press, 392pp.

Matsui, I., H. Kubomura, H. Imoto, and N. Sugimoto, 1994: Eye-safe compact Mie scattering lidar using a diode-laser-pumped Nd:YAG laser for measuring the atmospheric boundary layer. *Japanese J. Applied Physics*, **33**, 6569-6571.

Melles-Griot, Inc., 1995: **1995-1996 Catalogue**, Melles-Griot, pages 13-26 - 13-31.

Mesmer, H., 1994: **The Indispensable PC Hardware Book**, Addison-Wesley, 985 pp.

Oliver, J., T. O. Regan, H. C. Fenker, and J. Thomas, 1993: A method to quench and recharge avalanche photo diodes for use in high rate situations. *Nuclear Instruments and Methods in Physics Research*, **A326**, 570-573.

Omega Engineering, Inc., 1994: **CIO-DIO24 User's Manual**, Omega Engineering, 26 pp.

Omega Engineering, Inc., 1993: **CN76000 Microprocessor-based Temperature/Process Controller Operator's Manual**, Omega Engineering, 23 pp.

Omega Engineering, Inc.,1992: **Solid State Relay Operator's Manual**, Omega Engineering, 24 pp.

Schroeder, D. J., 1987: **Astronomical Optics**, Academic Press, 352 pp.

Spectra-Physics, Inc., 1994: **Model 7300 Laser Systems Instruction Manual**, Spectra-Physics, 58 pp.

Spinhirne, J. D., 1993: Micro Pulse Lidar. *IEEE Trans. Geoscience and Remote Sensing*, **31**, 48-54.

Streetman, B. G., 1990: **Solid State Electronic Devices**, Prentice Hall, 462 pp.

Sun, X. and F. M. Davidson, 1992: Photon Counting with Silicon Avalanche Photodiodes. *J. Lightwave Technology*, **10**, 1023-1032.

Temer, R., 1997: Technical support from CVI Laser Corp. Telephone conversation on February 12, 1997.

Walpole, R. E. and R. H. Myers, 1989: **Probability and Statistics for Engineers and Scientists**, Macmillan Publishing, 765 pp.

Willams, C. S. and O. A. Becklund, 1972: **Optics: A Short Course for Engineers and Scientists**, Wiley-Interscience, 397 pp.

Young, S. A., 1995: Analysis of lidar backscatter profiles in optically thin clouds. *Applied Optics*, **34**, 7019-7031.

Appendix A

MICRO PULSE LIDAR OVERLAP CORRECTION ALGORITHM

Background: Overlap signature is the signal degradation in the near range caused by field of view conflicts in the transmitter-receiver system.

Assumptions: 1) Need a MPL profile where the aerosol backscatter is constant throughout (ie: a horizontally aimed profile).
2) At some range, r_0, the overlap ceases to exist and the correction factor becomes 1.0.

Procedure: From the lidar equation, the range-corrected signal, P(r), can be defined as:

$$P(r) = [n(r) - n_b]r^2 = O_c(r)CE\beta(r)T^2 \quad (1)$$

where n(r) equals the measured signal return in photo electron counts per second at range r, n_b is a measured background signal from daytime solar photons entering the receiver, $O_c(r)$ is the overlap correction as a function of range, C represents a dimensional system calibration constant, E equals the laser pulse energy, $\beta(r)$ is the backscatter cross section due to all types of atmospheric scattering, and T is atmospheric transmittance. Knowing that $T=e^{-\tau}$ and $\tau=\sigma r$, where τ is optical thickness and σ is the extinction cross section, you can rewrite eq. (1) as:

$$P(r) = O_c(r)CE\beta(r)e^{-2\sigma r} \quad (2)$$

For the section of the profile where $r > r_0$ and $O_c=1.0$, take the natural log of both sides of eq. (2):

$$\ln[P(r)] = \ln[CE\beta(r)] - 2\sigma r \quad (3)$$

Using assumpton 1, $CE\beta(r)$ becomes a constant and plotting ln [P(r)] verses r takes the form of y=a+bx with -2σ as b (see accompanying figure). Next, simply do a line fit to the points where $r > r_0$ and calculate the slope value of -2σ. Solving eq. (2) for O_c, we have:

$$O_c(r) = \frac{P(r)}{CE\beta(r)e^{-2\sigma r}} \quad (4)$$

As referred to in eq. (3), $CE\beta(r)$ is assumed to be constant at all values of r in this special horizontal profile, so solving for $CE\beta(r)$ at $r > r_0$ where $O_c(r)=1.0$ shows:

$$CE\beta(r) = \frac{P(r)}{e^{-2\sigma r}} \quad (5)$$

Plugging this calculated value of $CE\beta(r)$ back into eq. (4) will then provide the overlap correction as a function of r for $r < r_0$.

MICRO PULSE LIDAR
OVERLAP CORRECTION USING HORIZONTAL PROFILE

*** Key Assumption - Aerosol Backscatter is constant throughout profile.**

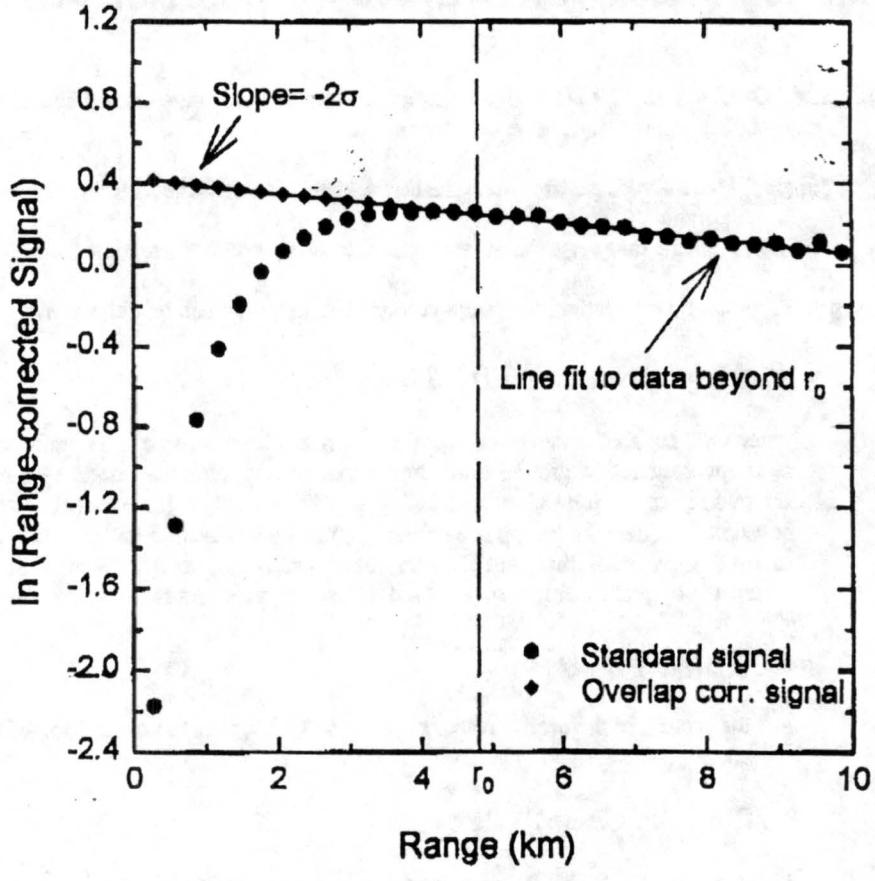

APPENDIX B

DETECTOR AFTERPULSING

During initial testing of the EG&G SPCM-AQ detector module, it was discovered that the blanking circuit was causing afterpulsing about 230 ns after releasing the gate as is observed in the figure below. After the design was changed at CSU's insistence, the problem was corrected. However, a small amount still occurs about 66 ns after the gating circuit is deactivated. It was agreed that this small amount is acceptable.

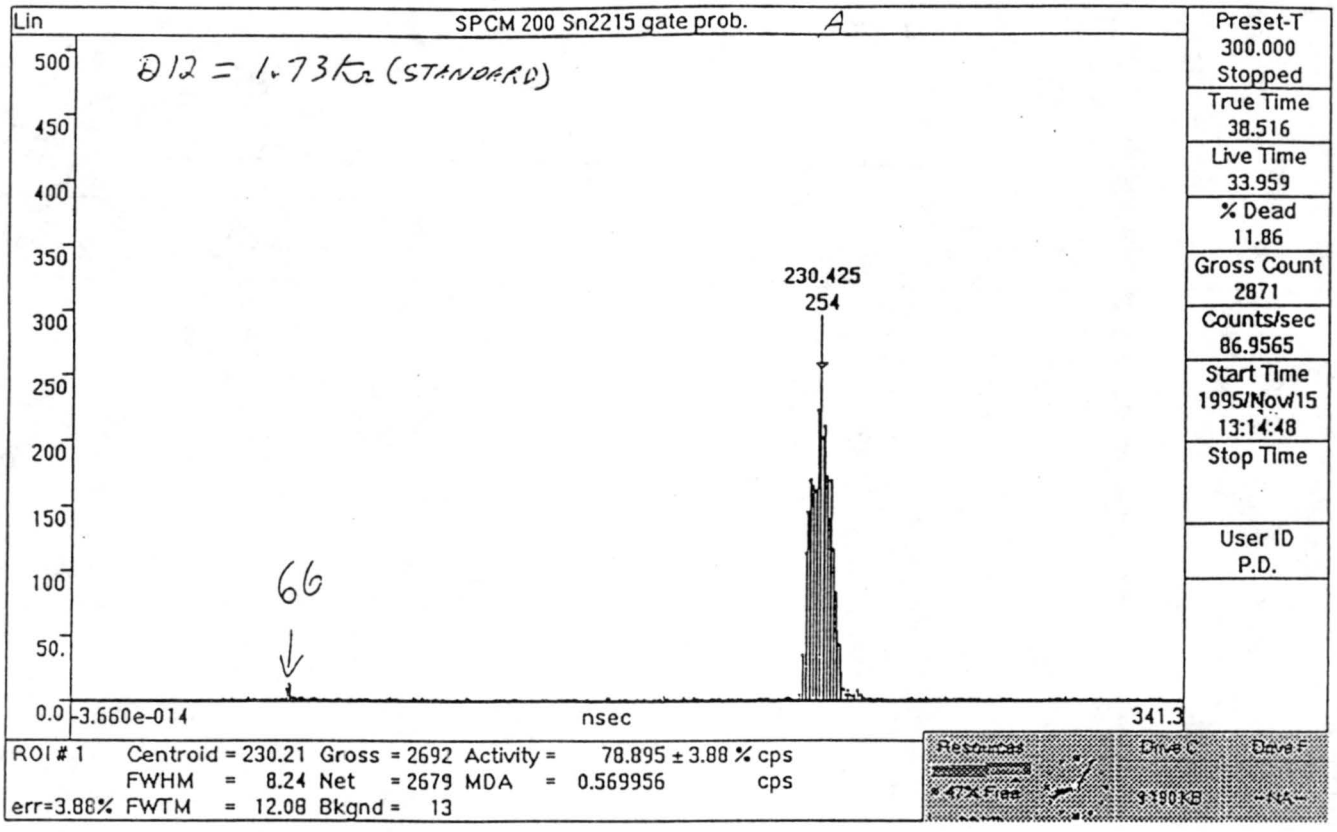

BEFORE

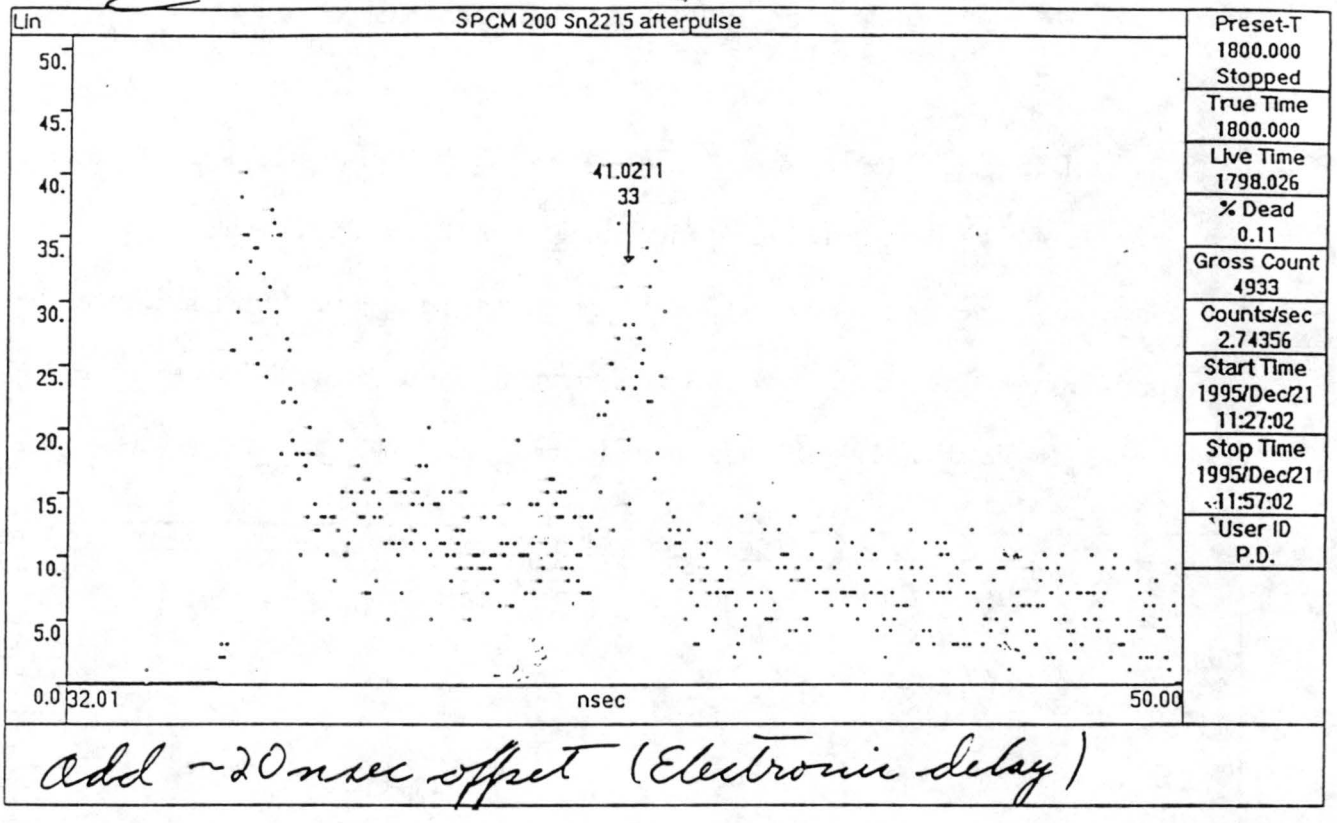

add ~20nsec offset (Electronic delay)

Appendix C

SAMPLE FRAME DUMP

The following is an example of the file produced by performing a frame dump.

Frame 25 of cfld0016.mpl.
Data taken 01\30\97 at 12:05:00

Number of range gates: 1024
Range gate spacing: 30
First range gate: 108
Pulse Repetition Frequency: 2500
Number background integrations: 62500
Number data integrations: 250000
Pulse energy: 0.0000E+000
Detector temp: 0.00
Filter temp: 48.00
Enclosure temp: 0.00
Laser temp: 0.00

R	BGND	BKSC
108	73	5278
138	75	4553
168	79	3940
198	69	3537
228	61	3172
.	.	.
.	.	.
30768	69	306
30798	68	312

Appendix D

INITIALIZATION FILE

The following is a typical MPLSYS.INI initialization file.

```
; MPLSYS.INI - initialization file for MPLCSU.EXE
; NOTE:  Keep initializers in this order.
;
[SST]
PRF = 2500          ;pulse repetition frequency
SPS = 20            ;seconds for a backscatter scan
NSPS = 5            ;seconds for a background scan
NCYC = 5            ;number of sets per frame
Q2P = 0.8           ;Q2P delay in microseconds
BLANK = 1.2         ;BLANK time in microseconds
B2A = 120.0         ;delay for ACQ from BLANK in nanoseconds

[MCS]
DWELL = 2.0000E-007         ;channel width in seconds
CHANNELS = 1024             ;number of channels
PASSES = 0                  ;passes = 0; externally controlled
SUM = 1                     ;sum instead of replace data
EXTTRIG = 1                 ;external (or internal) trigger
DISCEDGE = 1                ;count on leading (or falling) edge
THRESH =  0.999756          ;threshold voltage
DTMLPARM = 2.3340E-001      ;deadtime ML estimator factor

[LASER]
PUMP = 2.0          ;pump power in watts
REMOTE = 1          ;remote (or system) operation

 [UPDATE]
HOURS = 0           ;new frame every h hours
MINUTES = 4         ;           and m minutes
SECONDS = 0         ;           and s seconds
```

```
[DATA]
GATES = 1024        ;number of range gates to store in file

[FNAMES]
PREFIX = cfld       ;automatic file name generator.  Start with prefix and
NUMBER = 10         ;number and suffix with ".mpl."  This example would produce
                    ;cfld0010.mpl.  The number is then automatically
                    ;incremented.
```

Appendix E

DATA FILE FORMAT

The first byte in a data file is a "Magic Number" 95 (hexadecimal) which identifies the file as originating from the EMPL. Then, frames are stored in binary form using the following conventions,

BYTE	An 8-bit unsigned integer
WORD	A 16-bit unsigned integer
DWORD	A 32-bit unsigned integer
FLOAT	A 32-bit floating point value.

The frame data are stored in the following order:

BYTE year.
BYTE month.
BYTE day.
BYTE hours.
BYTE minutes.
BYTE seconds.
WORD number of range gates.
WORD gate spacing in meters.
WORD first gate height in meters.
WORD pulse repetition frequency in Hertz.
DWORD number of background integrations.
DWORD number of backscatter integrations.
FLOAT laser energy in microjoules.
FLOAT detector temperature in degrees Celsius.
FLOAT filter temperature in degrees Celsius.
FLOAT OTA enclosure temperature in degrees Celsius.
FLOAT laser temperature in degrees Celsius.
DWORD background data for all gates.
DWORD backscatter data for all gates.

Appendix F

PHOTOGRAPHS

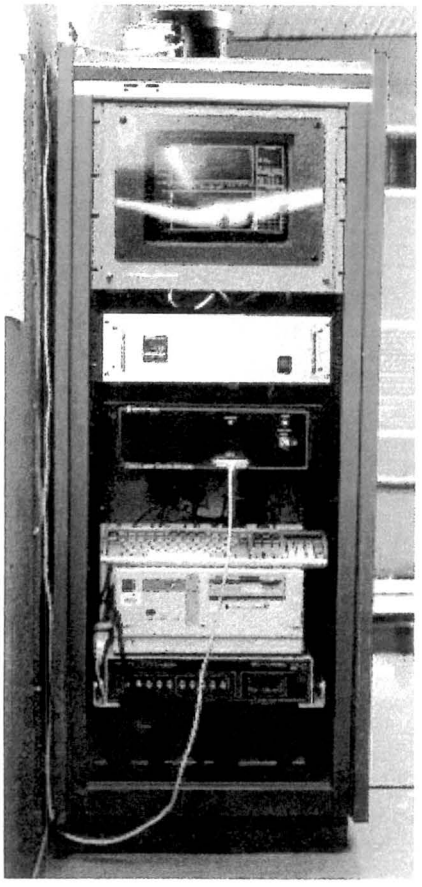

Figure F.1 - The EMPL system.

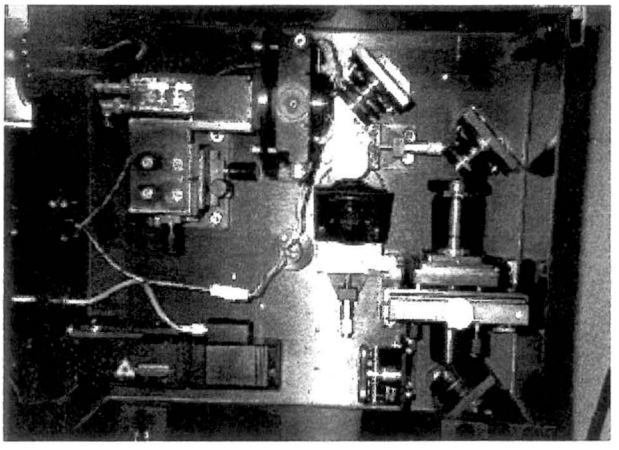

Figure F.2 - The OTA optics.

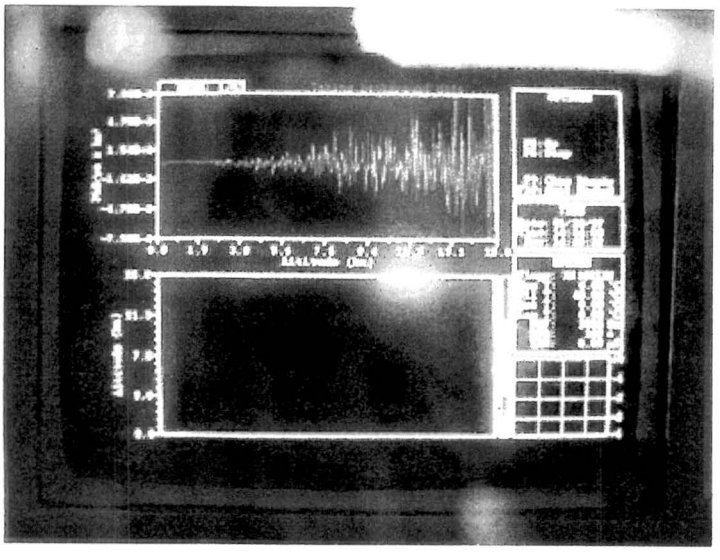

Figure F.3 - The EMPL display

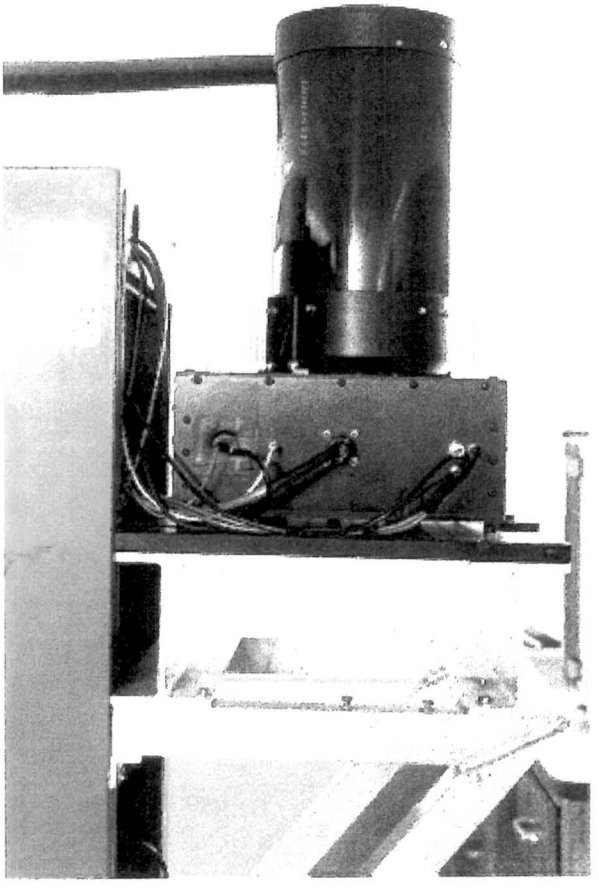

Figure F.4 - The Optical Transceiver Assembly.